NATIONAL ADVISORY COMMITTEE FOR AERONAUTICS

TECHNICAL MEMORANDUM 1198

INVESTIGATIONS ON THE STABILITY, OSCILLATION, AND STRESS CONDITIONS OF AIRPLANES WITH TAB CONTROL

SECOND PARTIAL REPORT - APPLICATION OF THE SOLUTIONS OBTAINED IN THE FIRST PARTIAL REPORT TO TAB-CONTROLLED AIRPLANES

By B. Filzek

Translation of ZWB Forschungsbericht Nr. 2000/2, November 1944

Washington
September 1949

NATIONAL ADVISORY COMMITTEE FOR AERONAUTICS

TECHNICAL MEMORANDUM 1198

INVESTIGATIONS ON THE STABILITY, OSCILLATION, AND STRESS CONDITIONS OF AIRPLANES WITH TAB CONTROL

SECOND PARTIAL REPORT – APPLICATION OF THE SOLUTIONS OBTAINED IN THE FIRST PARTIAL REPORT TO TAB-CONTROLLED AIRPLANES*

By B. Filzek

ABSTRACT: The first partial report, FB 2000, contained a discussion of the derivation of the equations of motion and their solutions for a tab-controlled airplane; the results obtained there are now to be applied to the longitudinal motion of tab-controlled airplanes.

In view of the abundance of structural factors and aerodynamic parameters, a general discussion of the problems is unfeasible. Thus it is demonstrated on the basis of examples what stability, oscillation, and stress conditions are to be expected for tab-controlled airplanes.

OUTLINE:

---

*"Untersuchungen über die Stabilitäts-, Schwingungs- und Beanspruchungsverhältnisse von Flugzeugen mit Hilfsrudersteuerung. 2. Teilbericht. Anwendung der im 1. Teilbericht gewonnenen Lösungen auf hilfsruder-gesteuerte Flugzeuge." Zentrale für wissenschaftliches Berichtswesen der Luftfahrtforschung (ZWB) Forschungsbericht Nr. 2000/2, November 15, 1944. This translation is the second partial report (2. Teilbericht) of an investigation made up of two parts, the first part, FB 2000, 1. Teilbericht of which is NACA TM 1197.

I. INTRODUCTION

The mathematical relations obtained in FB 2000 now offer the expedients to determine and evaluate the phenomena of motion to be expected for tab controls. Aside from stability discussions special attention will be paid to the starting phenomena in "control displacement" and "control restoration" with the resulting stresses.

For these investigations the airplane is regarded as a rigid body. This presupposition is only conditionally fulfilled. Periodic excitations of the tabs due to form variations caused by external forces, for instance engine vibrations or gusts, are imaginable which can exclude flying with "free control surface" and must, therefore, be investigated separately.

For the determination of the system constants [17][1] one will use tunnel results for the aerodynamic coefficients of the wing and horizontal tail $\frac{\partial C_a}{\partial \alpha}$ $\frac{\partial C_{MF}}{\partial \alpha}$, etc. As far as such results do not exist, one will in designing an airplane have to go back to the theory.[2]

If the form of one parameter $^{(1)}a_{1\eta}$ is selected for the main control surface damping, it is supposed to take the damping due to air forces into consideration as well as eventual additional mechanical damping.

---

[1]It is noted that the numbering of the formulas and figures is continued conforming to the first partial report and that data in brackets refers to it.

[2]Bibliography, (5) and (9).

II. SYMBOLS

The symbols used correspond to the German standards DIN L 100 second edition, July 1939; moreover the following designations are selected (see also fig. [1]):

m	mass of the entire airplane
m_1	partial mass fuselage without control surfaces and tabs
m_2	partial mass control surfaces without tabs
m_3	partial mass tabs
S	center of gravity of the whole system
S_1	center of gravity of the partial masses m_1
S_2	center of gravity of the partial masses m_2
S_3	center of gravity of the partial masses m_3
e_1	distance of the center of gravity of the partial mass m_1 from the center of gravity of the whole system
e_2	distance of the center of gravity of the partial mass m_2 from the center of rotation of the main control surface
e_3	distance of the center of gravity of the partial mass m_3 from the center of rotation of the tab
F_y	moment of inertia of the entire airplane about y-axis
F_{S_1}	moment of inertia of the partial mass m_1 about y-axis through S
F_{S_2}	moment of inertia of the partial mass m_2 about S_2
F_{S_3}	moment of inertia of the partial mass m_3 about S_3
F_{Hr}	moment of inertia of the elevator about axis of rotation of the main control surface

F_{Hh} moment of inertia of tab about axis of rotation of tab

η_h deflection of the tab

$\Delta\eta_{hmax}$ deflection of the tab required for attaining the safe multiple of load

l_{Hr} chord of the elevator + tab

l_{Hh} chord of the tab

C_{MF} coefficient of the air force moment of the airplane without horizontal tail referred to center of gravity of the airplane

C_{nH} coefficient of the normal force of the horizontal tail

C_{mH} coefficient of the horizontal tail moment referred to the axis through the aerodynamic center of the horizontal tail parallel to the y-axis

C_{rH} coefficient of the elevator moment referred to the axis of rotation of the main control surface

C_{rHh} coefficient of the tab moment referred to the axis of rotation of the tab

α_H angle of attack at the location of the horizontal tail

q_H mean dynamic pressure at the location of the horizontal tail

v_H mean velocity at the location of the horizontal tail

Δ mean downwash angle at the location of the horizontal tail

δ_H ratio of the air force damping of the entire airplane with respect to lateral axis to the air force damping of the horizontal tail

If similar symbols appear in the individual paragraphs (for instance $\Delta\alpha$ = angle-of-attack increment, ΔM_ζ = moment increment, Δ = downwash angle, Δ_K = determinant, Δ^* = Routh's discriminant), they are distinguished by indices and their significance follows from the respective connection.

III. PRESUPPOSITIONS

In order to circumscribe the range of validity of this report the necessary presuppositions shall be mentioned in advance once more.

1. Unsteady air force influences are not taken into account.

2. Flight motions are possible only in the $X_g Z_g$ plane.

3. Method of small oscillations.

4. Fully compensated control surfaces, that is, the centers of gravity lie on the axes of rotation of the control surfaces.

5. Omission of the mass couplings and horizontal tail surface forces in the force equations.

6. Omission of the mass couplings and of the force couple at the horizontal tail at $C_{aH} = 0$ (zero moment) in the equation of moments about the lateral axis.

7. The velocity along the flight path v for the phenomenon under consideration is assumed to be constant.

8. Air forces and moments are assumed to be linear functions of their variables.

9. The steady state about which the system oscillates is assumed to be horizontal flight.

10. The dynamic pressure ratio $\frac{q_H}{q}$ and the downwash factor $\frac{\partial \Delta}{\partial \alpha}$ are regarded as constant during the flight motions.

11. The airplane framework is regarded as a rigid body.

IV. APPLICATION OF THE SOLUTIONS OBTAINED IN FB 2000 TO TAB-CONTROLLED AIRPLANES

1. Stability and Frequency Behavior.

With regard to flight safety one will always have to stipulate a minimum measure of stability.

The necessary and sufficient condition for a stable system of motion is the requirement that the real roots and the real parts of the complex roots of the characteristic equation $D(p) = 0$ [53] are negative[3], that is,

$$R(p_\mu) < 0 \tag{70}$$

If it is merely a matter of determining whether the system is stable or unstable and no data on the magnitude of these quantities are required, the conditions[4] are sufficient that all coefficients of the characteristic equation $D(p) = 0$ [53] and Routh's discriminant[5] are positive. Thus the conditions have to be satisfied

$$\left.\begin{aligned} &a_\mu > 0 \\ &\Delta^* = \begin{vmatrix} a_3 & 1 & 0 \\ a_1 & a_2 & a_3 \\ 0 & a_0 & a_1 \end{vmatrix} > 0 \end{aligned}\right\} \tag{70a}$$

This formulation (70a) of the stability conditions is very useful for the designing of airplanes. It permits stability limits to be indicated and the influence of structural and aerodynamic quantities to be varied so that stability is guaranteed.

With the conditions (70) and (70a), respectively, taken as basis it is customary to speak of dynamic stability, whereas one regards as measure for the static stability the condition that the coefficient a_0 of the characteristic equation $D(p) = 0$ [53] is positive,

or

$$a_0 > 0 \tag{70b}$$

From the formulation of (70a) follows that for ensuring of the dynamic stability the existence of static stability is required but <u>not</u> sufficient.

Even though the definition of static stability may be useful for dynamic systems with one degree of freedom it is shown by what was said above that the importance of the static stability lessens for dynamic systems with several degrees of freedom.

---

[3]Bibliography (7)
[4]Bibliography (7)
[5]Bibliography (1), (2), (7)

However, if it is a matter of investigating starting phenomena, it is always necessary, in order to obtain the solutions found in FB 2000, to know the roots p_μ of the characteristic equation $D(p) = 0$ [53]. However, in that case one will go back to the definition (70) and be able to discuss stability as well as frequency conditions for the parameters which appear to have the greatest influence on the various problems stated. If one chooses, therefore, the method of solving equations of the fourth degree and plots real as well as imaginary part of the roots p_μ as functions of these parameters, one gains a rather good over-all view.

a. Variable main control surface damping.

Figure 7 shows the conditions for an airplane (Fl_1) for full permissible load and variable main control surface damping.

Since the real parts are $R(p_\mu) < 0$ the system is always stable. With increasing control surface damping the frequency ω_1 decreases in a form similar to a parabola until it becomes zero for the aperiodic case. Shortly ahead of it lies the position of resonance, that is, the angular frequencies ω_1 and ω_2 are equal. It may be mentioned at this point that, due to the strong control surface damping, this position is of no particular significance. The frequency ω_2 and damping constant κ_2 show in this interval only slight variations.

The fact should be emphasized that a control surface damping occurs also when ${}^{(1)}a_{1\eta} = 0$ which can be traced back to the coupling term ${}^{(1)}a_{1\dot{\alpha}}\,\alpha'$ in [17a].

However, an airplane must be airworthy for any permissible load. The results of calculation for the empty airplane are given in figure 8. Here, too, $R(p_\mu) < 0$ and therewith the stability of the system is ensured. ω_1 and κ_1 show a similar course as in figure 7; however, it is conspicuous that no ω_2 but instead two κ_2 are present and permit a conclusion as to a dynamic stability increasing with decreasing flying weight.

b. Variable masses of control surfaces for equal contour.

If one visualizes once more the third equation of [6c]

$$\left[F_{Hr} + m_3 r_H (l_{Hr} - l_{Hh})\right]\ddot{\vartheta} + F_{Hr}\ddot{\eta} = M_{Hr}$$

the influence of the coupling term due to the mass of the tab $m_3 r_H(l_{Hr} - l_{Hh})$ will justifiably be questioned; the following two cases will be investigated:

α. The main control surface remains unvaried while the mass of the tab is varied.

With Steiner's theorem taken into account, the equation

$$F_{Hr} = F_{2Hr} + \lambda_1 m_3 (l_{Hr} - l_{Hh})^2 + F_{Hh} \tag{71}$$

is valid, F_{2Hr} signifying the moment of inertia of the mass m_2 about the axis of rotation of the main control surface, F_{Hh} the moment of inertia of the mass m_3 about the axis of rotation of the tab.

If (71) is introduced into the coefficient of ϑ, there results, if one puts in first approximation $F_{Hh} \cong 0$

$$F_{Hr} + \lambda_1 m_3 r_H (l_{Hr} - l_{Hh}) = F_{2Hr} + \lambda_1 m_3 (l_{Hr} - l_{Hh})(r_H + l_{Hr} - l_{Hh}) \tag{72}$$

Figure 9 shows the components of the roots p_μ of the characteristic equation $D(p) = 0$ [53] for an airplane type (Fl_2).

β. The tab remains constant while the moment of inertia of the main control surface is varied.

For this assumption the expression

$$F_{Hr} = \lambda_2 F_{2Hr} + m_3 (l_{Hr} - l_{Hh})^2 + F_{Hh} \tag{73}$$

is proper, and it follows with $F_{Hh} \cong 0$

$$F_{Hr} + m_3 r_H (l_{Hr} - l_{Hh}) = \lambda_2 F_{2Hr} + m_3 (l_{Hr} - l_{Hh})(r_H + l_{Hr} - l_{Hh}) \tag{74}$$

Figure 10 illustrates the result.

In both cases the $R(p_\mu)$ remain less than zero so that the stability of the system is not endangered. It is noteworthy that, whereas the frequencies ω_1 and ω_2 decrease with the increase of the moment of

inertia of the main control surface F_{2Hr} (fig. 10), with increasing mass m_3 of the tab, an increase of the frequency ω_1 takes place (fig. 9).

2. Starting Phenomena for Instantaneous and Time-Dependent Tab Control.

The results obtained in the previous paragraph do not yet procure an insight into the kinetic phenomena of a tab-controlled airplane. A general discussion of the solutions derived in FB 2000 is not feasible with the mathematical connections being no longer quite simple. Thus already the determination of the maxima of the main control surface deflection $\Delta\eta_{max}$ and of the angle of attack $\Delta\alpha_{max}$ requires the solution of transcendental equations. If a numerical expenditure is necessary anyway, it seems best to forego the determination of selected points of the course of motion and to represent the entire phenomenon of motion as a function of time. Thus one obtains the possibility of comparing not only individual points, but entire sudden-deflection phenomena.

a. Control displacement.

In flight practice control-displacement motions, for instance in landing or in "zooming in front of an obstacle", are of particular importance when catastrophes are to be avoided. Thus the designer will endeavor to develop the control effectiveness of the control surfaces in such a manner that losses are excluded in case of purposeful control maneuvering. First, once the conditions for direct activation of the control organs are clarified, one must not overlook what effectiveness is to be expected and attainable for indirect tab control. Figure 11 shows a comparison of the following deflection phenomena of the control surfaces:

1. Instantaneous deflection of the tabs.

2. Tab deflection as linear time function.

3. Instantaneous deflection of the main control surfaces.

4. Main-control-surface deflection as linear time function.

For the latter two phenomena one must visualize the auxiliary control surface as blocked. Thereby appears, in comparison with indirect sudden deflection, a larger C_{aH}-variation at the horizontal tail so that a smaller deflection of the main control surface $\Delta\eta$ is sufficient for obtaining an equal variation in angle of attack $\Delta\alpha$. If one analyzes, at first, the first two deflection phenomena (fig. 11) it is conspicuous that in spite of the small main control surface damping selected $^{(1)}a_{1\eta} = 0.15$ (cf. fig. 7) the control surface oscillation is damped very rapidly. In the variation of the angle of attack an oscillation is hardly recognizable.

For time-dependent tab deflection the time required for the deflection of the tabs $\tau_{s\ max}$ with the relation $\tau_{s\ max} = t_s\sqrt{q_{max}}$ was fixed so that for the highest flight dynamic pressure q_{max} the tab assumes the deflection required for attainment of the safe multiple of load in about $t_s = 0.1$ second. As a consequence, longer and longer periods of time required for deflection t_s correspond, with decreasing dynamic pressure, to equal $\tau_{s\ max}$. If, however, one makes the requirement that for instance for the lowest dynamic pressure q_{min} the deflection time also should be $t_s = 0.1$ second there follows from the relation

$$\lim_{q_{min} \to 0} \tau_s = \lim_{q_{min} \to 0} \sqrt{q_{min}}\ t_s = 0$$

that with decreasing dynamic pressure the deflection phenomenon approaches the case of instantaneous tab deflection.

As figure 11 shows, the $\Delta\alpha$-curves for both phenomena differ even for $\tau_{s\ max}$ practically only by a parallel displacement of $\Delta\tau_3$, and it remains to be investigated what effects are caused thereby.

First, the deflection phenomena for direct main control surface activation will be discussed. Obviously instantaneous main control surface deflection represents the upper limit of what may be attained and is illustrated by the fullest $\Delta\alpha$-curve (3 in fig. 11). For linear main control surface deflection the deflection velocity was selected so as to be equal to the maximum deflection velocity due to instantaneous tab activation. Whereas the two $\Delta\alpha$-curves show for direct main control surface deflection immediately positive increments, the $\Delta\alpha$-curves become for tab activation, due to the C_{a_H}-decrease at the horizontal tail by the tab deflection which corresponds to a control reversal, at first negative and then also positive.

The displacements with time of the individual $\Delta\alpha$-curves could be visualized also as brought about by control displacement with control surfaces of different effectiveness. As measure of the control effectiveness one may regard the time required to exceed a difference in altitude $Z_g - Z_{go} = \Delta Z_g$ yet to be fixed.

To this the following deliberations:

From the relation [13]

$$\frac{d\gamma}{dt} = \frac{\partial C_a}{\partial \alpha} \frac{F}{G} g \sqrt{\frac{\rho}{2} q_o}\, \Delta\alpha(t)$$

or with the independent variable $\tau = \sqrt{q_o}\, t$

$$\frac{d\gamma}{dt} = \frac{d\gamma}{d\tau} \frac{d\tau}{dt} = \frac{\partial C_a}{\partial \alpha} \frac{F}{G} g \sqrt{\frac{\rho}{2} q_o}\, \Delta\alpha(\tau) \frac{\Delta\eta_{hmax}}{\Delta\eta_{hmax}}$$

follows

$$\frac{\Delta\gamma}{\Delta\eta_{hmax}} = \frac{\partial C_a}{\partial \alpha} \frac{F}{G} g \sqrt{\frac{\rho}{2}} \int_{0}^{\tau} \left\{ \frac{\Delta\alpha(\zeta)}{\Delta\eta_{hmax}} \right\} d\zeta \tag{75}$$

With the assumptions of small variations and $v = \text{const.} = v_o$ the third equation of the relations connecting the variables [5]

$$\tan \gamma = \frac{Z_g}{x_g}$$

may also be written

$$\Delta\gamma = \frac{\dot{Z}_g}{v_o}$$

or, taking the substitution $\tau = \sqrt{q_o}\, t$ into account,

$$\frac{dZ_g}{dt} = \frac{dZ_g}{d\tau} \frac{d\tau}{dt} = \Delta\gamma v_o$$

or

$$\frac{dZ_g}{d\tau} = \Delta\gamma \sqrt{\frac{2}{\rho}} \frac{\Delta\eta_{hmax}}{\Delta\eta_{amax}},$$

respectively. Then one obtains

$$\frac{\Delta Z_g}{\Delta\eta_{hmax}} = \sqrt{\frac{2}{\rho}} \int_0^\tau \left\{ \frac{\Delta\gamma(\zeta)}{\Delta\eta_{hmax}} \right\} d\zeta$$

or, because of (75),

$$\frac{\Delta Z_g}{\Delta\eta_{hmax}} = \frac{\partial c_a}{\partial\alpha} \frac{F_g}{G} \int_0^\tau d\zeta \int_0^\zeta \left\{ \frac{\Delta\alpha(\zeta)}{\Delta\eta_{hmax}} \right\} d\zeta \tag{76}$$

The changes in altitude compared to an initial flight altitude Z_{go} which can be attained with the aid of the double integration (76) are represented in figure 12. From the condition that all $\Delta\alpha$ approach, for different deflection phenomena, an equal limiting value follows that the curves for $\tau > 70$ (cf. also fig. 11) are displaced parallel to each other. However, the deviation from parallelism is insignificant also for $\tau < 70$.

If one regards the time $\tau_{\eta_{h\ time-dep.}}$ for time-dependent tab deflection which is required for attainment of a certain difference in altitude ΔZ_g, as measure of reference, the gain in control effectiveness due to the other possibilities of deflection may be expressed by the relation

$$W_v = \frac{\Delta\tau_v}{\tau_{\eta_{h\ time-dep.}}} \tag{77}$$

plotted in figure 13. One recognizes that the increase in control effectiveness is rather considerable for small τ; it decreases, however, the more the longer one succeeds in keeping the angle-of-attack variation $\Delta\alpha$ constant (cf. fig. 11).

In flight practice, however, only that time will have to be especially considered where $\Delta\alpha$ attains the maximum, that is in this example $50 < \tau < 60$; from figure 13 can be seen that then the increase in control effectiveness as compared to time-dependent tab deflection does not exceed the limits

4 % for instantaneous tab deflection
12.5 % for time-dependent main control surface deflection
20 % for instantaneous main control surface deflection

These explanations show that the assumed deflection velocity of the tab has an insignificant influence on the course of motion. Thus it does not imply an essential restriction if the further investigations are based on instantaneous tab deflection.

b. Control restoration.

In order to end the control displacement or, respectively, to avoid unintended flight positions due to phenomena of flow separation the pilot will try to restore the airplane to normal position by opposite control measures.

Since at the moment τ_N of the control restoration the end values of the control displacement $\Delta\alpha(\tau_N)$, $\alpha'(\tau_N)$, $\Delta\eta(\tau_N)$ and $\eta'(\tau_N)$ denote the initial conditions of the control restoration, it is clear that the analytical description of the phenomenon becomes rather complex.

If one interprets, on the other hand, the control restoration as superposition of the two deflection phenomena (fig. 14)

$$\left.\begin{aligned} \Delta\eta_h &= \Delta\eta_h(\tau) && \text{for } 0 \leqq \tau < \infty \\ \text{and} & \\ \Delta\eta_h &= \begin{cases} 0 & \text{for } 0 \leqq \tau < \tau_N \\ -\Delta\eta_h(\tau - \tau_N) & \text{for } \tau_N \leqq \tau < \infty \end{cases} \end{aligned}\right\} \tag{78}$$

one obtains the corresponding solutions in the simplest manner by graphical subtraction without determination of the initial conditions.

The solutions for $\Delta\alpha$ and $\Delta\eta$ thus obtained are compiled in figures 15 to 17 for the times of control restoration $\tau_N = 60, 30, 15, 10$ and allow insight into the kinetic phenomena.

3. Wing and horizontal tail stresses.

With respect to the structural aspects, the designer is interested, apart from the flight-mechanical properties, in the resultant stresses.

The stresses in the wing unit caused by control displacement are given with the relation

$$nG = \frac{\partial C_a}{\partial \alpha} q_o F(\alpha_o + \Delta\alpha)$$

Since for the steady horizontal flight

$$G = \frac{\partial C_a}{\partial \alpha} q_o F \alpha_o$$

is valid, there follows for the additional multiple of load due to the variation in angle of attack

$$\frac{\Delta n}{q_o \Delta \eta_{hmax}} = \frac{\partial C_a}{\partial \alpha} \frac{F}{G} \frac{\Delta \alpha}{\Delta \eta_{hmax}} \tag{79}$$

Thus the additional multiple of load referred to the dynamic pressure and the tab deflection is directly proportional to the functions of the $\Delta\alpha$-coordinate represented in figures 15 to 17; the scale has to be multiplied by the factor $\frac{\partial C_a}{\partial \alpha} \frac{F}{G}$.

For the proportioning of fuselage and horizontal tail the horizontal tail load P_H is to be regarded as decisive.

The second equation of [6c] reads, if [8] and [15] are taken into consideration,

$$F_y \ddot{\vartheta} = \frac{\partial C_{MF}}{\partial \alpha} qF l \, \Delta\alpha - \left\{ \frac{\partial C_{nH}}{\partial \alpha_H} \left[\left(1 - \frac{\partial \Delta}{\partial \alpha} \right) \Delta\alpha + \frac{r_H}{v_H} \frac{\partial \Delta}{\partial \alpha} \dot{\alpha} + \frac{r_H}{v_H} \delta_H \dot{\vartheta} \right] \right.$$

$$\left. + \frac{\partial C_{nH}}{\partial \eta} \Delta\eta + \frac{\partial C_{nH}}{\partial \eta_h} \Delta\eta_h \right\} qF_H r_H \frac{q_H}{q}$$

If one transforms this condition of moment equilibrium about the center of gravity of the airplane so that the moment of the horizontal tail load balances all other moments

$$\Delta P_H r_H = \left\{ \frac{\partial C_{nH}}{\partial \alpha_H} \left[\left(1 - \frac{\partial \Delta}{\partial \alpha} \right) \Delta\alpha + \frac{r_H}{v_H} \frac{\partial \Delta}{\partial \alpha} \alpha + \frac{r_H}{v_H} \vartheta \right] + \frac{\partial C_{nH}}{\partial \eta} \Delta\eta + \frac{\partial C_{nH}}{\partial \eta_h} \Delta\eta_h \right\} qF_H r_H \frac{q_H}{q}$$

$$= \frac{\partial C_{MF}}{\partial \alpha} qF l \, \Delta\alpha - \frac{\partial C_{nH}}{\partial \alpha_H} \left(\delta_H - 1 \right) qF_H r_H \frac{q_H}{q} \vartheta - F_y \ddot{\vartheta}$$

there follows for the increment (referred to the dynamic pressure and the tab deflection) of the horizontal tail load as compared to the steady horizontal flight, with [16] taken into consideration, the expression

$$\frac{\Delta P_H}{F_H q\, \Delta\eta_{hmax}} = h_o \frac{\Delta\alpha}{\Delta\eta_{hmax}} + h_1 \frac{\alpha}{\Delta\eta_{hmax}} + h_2 \frac{\Delta\eta}{\Delta\eta_{hmax}} + h_3 \frac{\Delta\eta_h}{\Delta\eta_{hmax}} \tag{80}$$

with the coefficients

$$\left.\begin{aligned} h_o &= \frac{\partial C_{nH}}{\partial\alpha_H}\frac{q_H}{q}\left[1 - \frac{\partial\Delta}{\partial\alpha} + \frac{\partial C_a}{\partial\alpha}\frac{F}{G}\, g\, \frac{\rho}{2}\, r_H \sqrt{\frac{q}{q_H}}\right] \\ h_1 &= \frac{\partial C_{nH}}{\partial\alpha_H}\frac{q_H}{q}\frac{r_H}{v_H}\left(1 + \frac{\partial\Delta}{\partial\alpha}\right) \\ h_2 &= \frac{\partial C_{nH}}{\partial\eta}\frac{q_H}{q} \\ h_3 &= \frac{\partial C_{nH}}{\partial\eta_h}\frac{q_H}{q} \end{aligned}\right\} \tag{80a}$$

The determination of the horizontal tail load is once more performed most practically in graphical manner and is ascertained in figures 18 to 21 for the four types of control motion mentioned in section IV, 2a.

If one compares the occurring maximum horizontal tail loads ΔP_{H_1}, then the deflection phenomena $\Delta\eta_h$ instantaneous, $\Delta\eta_h$ time-dep., and $\Delta\eta$ time-dep. show about equal values whereas about 50 percent higher values are found for the assumption of instantaneous main control surface deflection.

With the aid of these figures, 18 to 21, it is possible to give immediately the variation of the horizontal tail loads in control restoration by applying the rule (78) at the times τ_N and superposing the solutions as was done in figures 22 to 25 for $\Delta\alpha$ and $\Delta\eta$.

In control restoration as in control displacement it is, in view of the structural aspects, not so much the variation with time that is of interest as the maxima ΔP_{H_2} of the horizontal tail loads for control restoration. Here also it proves advantageous to represent control displacement and restoration by two independent kinetic processes: If one visualizes the control restoration continuously at each time $\tau = \tau_N$, one obtains the envelope of all peak values ΔP_{H_2} by subtracting the peak value ΔP_{H_1} from the variation of curve representing the control displacement. These curves are drawn in dashed lines in figures 22 to 25; they make the determination of the absolute maximum possible which then forms the basis for the stress calculations. It is emphasized that the maximum for instantaneous main control surface deflection is for the value ΔP_{H_2} as well about 50 percent higher than for the other deflection phenomena which also differ only slightly.

4. Amplitude and Phase Displacement Functions.

At the end of this paragraph the amplitude and phase displacement functions obtained according to [64], which are represented in figures 26 to 29, will be discussed.

From the expression

$$\Delta\eta_h(\tau) = \Delta\eta_{hmax}\, e^{i\Omega\tau}$$

it follows that $\Omega = 0$ is identical with instantaneous tab deflection. Thus amplitude functions with $\Omega \to 0$ must tend toward the limiting value

$$\lim_{\tau \to \infty} \frac{\Delta\alpha}{\Delta\eta_{hmax}} = \frac{\Delta_2(0)}{D(0)} \quad \text{or} \quad \lim_{\tau \to \infty} \frac{\Delta\eta}{\Delta\eta_{hmax}} = \frac{\Delta_1(0)}{D(0)} \quad \text{respectively.}$$

If Ω increases indefinitely one can see from [64a] and [63a] that the curves converge towards zero, because the order of the numerator is smaller than that of the denominator.

In the neighbourhood of the normal frequency of the main control surface ω_η the curves V_1, V_2 show for small damping parameters ${}^{(1)}a_{1\eta}$ distinct maxima. For V_1 a weak maximum for ${}^{(1)}a_{1\eta} = 0$ also is recognizable in the neighbourhood of the normal frequency of the airplane ω_α, with ω_y and ω_x defined according to (82a) and (91a), respectively.

The reason for the V_1-curve for ${}^{(1)}a_{1\eta} = 0$ remaining limited is the aforementioned fact that the main control surface is always damped due to the coupling term ${}^{(1)}a_{1\dot{\alpha}}\alpha'$ (cf. figs. 7 and 8).

According to experiences so far, one will probably have to expect in flying practice, due to air forces, for the values ${}^{(1)}a_{1\eta}$ the order of magnitude $0.3 < {}^{(1)}a_{1\eta} < 0.5$. The amplitude curves then show that additional dampings do not become necessary.

Oscillations in the variation* of the angle of attack will no longer be measurable for $\Omega > 0.6$ although the $\Delta\eta$-coordinate still shows amplitudes of $\frac{V_1}{\Delta\eta_{hmax}} = 0.25$.

The phase displacement curves shown in figures 28 and 29 express that for $\Omega \to 0$ tab and airplane oscillation are in phase whereas tab and main control surface oscillation, due to aerodynamic coupling, are out of phase.

In the neighbourhood of the normal frequency of the main control surface the main control surface oscillation is lagging by about $3\pi/2$ compared to the tab oscillation, whereas the airplane oscillation is almost out of phase.

With $\Omega \to \infty$ tab, main-control-surface, and airplane oscillation are displaced by 2π, that is, they are in phase.

Small damping parameters ${}^{(1)}a_{1\eta}$ in the neighbourhood of the normal frequency of the main control surface ω_η attract attention by large phase increase.

In order to obtain a survey of the permanent state for periodic excitation of the tab, figure 30 shows for ${}^{(1)}a_{1\eta} = 0.15$ and $\Omega = 0.2$, that is, for an excitation in the neighbourhood of the normal frequency of the main control surface ω_η, the $\Delta\eta_h$-, $\Delta\eta$-, $\Delta\alpha$- and ΔP_H-variation against time.

---

*Translator's note: Literally "motion"

It must be stressed that the horizontal tail loads exceed the values for instantaneous main control surface deflection. Since, however, for the parameter $^{(1)}a_{1\eta}$ values between 0.3 and 0.5 are to be expected, the horizontal tail loads are reduced to about one half. Even if these reduced loads do not exceed the values due to control displacement or restoration, it will still be advisable to avoid periodic excitations because of fatigue.

V. APPROXIMATION METHOD FOR THE DETERMINATION OF THE WING AND HORIZONTAL TAIL STRESSES

For preliminary calculation of wing and horizontal tail stresses in airplane designing a calculation method will be desirable which is as far as possible simpler than that permitted by the exact solution with consideration of the two degrees of freedom $\Delta\alpha$ and $\Delta\eta$.

A comparison of figures 22, 23 and 25 shows that the maximum horizontal tail stress for instantaneous and time-dependent tab deflection differs only slightly from the value which results when the main control surface is deflected with according deflection velocity and amplitude. The deflection velocity should be chosen so as to be equal to the maximum main control surface deflection velocity due to tab deflection, whereas the amplitude is to be fixed so that an equal maximum multiple of load and thus equal wing stress are produced.

Figures 16 and 17 show that, up to the time τ_m of maximum deflection velocity of the main control surface, the α-coordinate will exert little influence on the course of motion of $\Delta\eta$. It will then be justified to put for the determination of the maximum deflection velocity of the main control surface in first approximation

$$\Delta\alpha = \alpha' = \alpha'' = 0$$

from the first equation of [17a] one obtains

$$\eta'' + {}^{(1)}a_{1\eta}\eta' + {}^{(0)}a_{1\eta}\Delta\eta = C_1\Delta\eta_h \tag{81}$$

The optimum main control surface deflection velocity is obviously attained for

$$\Delta\eta_h = \text{const.} = \Delta\eta_{h\max}$$

With this expression one obtains as solution of (81)

$$\frac{\Delta\eta}{\Delta\eta_{hmax}} = \frac{C_1}{(0)a_{1\eta}}\left[1 + \left\{\frac{\kappa_\eta}{\omega_\eta}\sin\omega_\eta\tau - \cos\omega_\eta\tau\right\}e^{\kappa_\eta\tau}\right] \tag{82}$$

with

$$\left.\begin{aligned}\kappa_\eta &= -\frac{(1)a_{1\eta}}{2}\\ \omega_\eta &= \sqrt{(0)a_{1\eta} - \left(\frac{(1)a_{1\eta}}{2}\right)^2}\end{aligned}\right\} \tag{82a}$$

Then the deflection velocity becomes

$$\frac{\eta'}{\Delta\eta_{hmax}} = \frac{C_1}{\omega_\eta}e^{\kappa_\eta\tau}\sin\omega_\eta\tau \tag{83}$$

and the second derivative

$$\frac{\eta''}{\Delta\eta_{hmax}} = \frac{C_1}{\omega_\eta}\left[\kappa_\eta\sin\omega_\eta\tau + \omega_\eta\cos\omega_\eta\tau\right]e^{\kappa_\eta\tau} \tag{84}$$

The deflection velocity reaches its maximum when $\eta'' = 0$, that is, when the condition

$$\kappa_\eta\sin\omega_\eta\tau_m + \omega_\eta\cdot\cos\omega_\eta\tau_m = 0$$

is satisfied, and there follows for

$$\tau_m = \frac{1}{\omega_\eta}\operatorname{arc\,tan}\left(-\frac{\omega_\eta}{\kappa_\eta}\right) \tag{85}$$

(85) substituted in (83) yields for the maximum deflection velocity the relation

$$\left(\frac{\eta'}{\Delta\eta_{hmax}}\right)_{max} = \frac{C_1}{\sqrt{(0)a_{1\eta}}} e^{\frac{\kappa_\eta}{\omega_\eta} \arctan\left(-\frac{\omega_\eta}{\kappa_\eta}\right)} \tag{86}$$

For preliminary calculations the main control surface variation will be idealized in such a manner that it increases linearily with (86) up to a maximum deflection $\Delta\eta_{max}$ and then remains constant (fig. 31). With this deflection phenomenon as a disturbance function the equation of motion of the α-coordinate from the second equation of [17a] obtains with $\Delta\eta_h = 0$ the form

$$\alpha'' + (1)a_{2\alpha}\alpha' + (0)a_{2\alpha}\Delta\alpha = -(0)a_{2\eta}\Delta\eta(\tau) \tag{87}$$

For $\tau \longrightarrow \infty$ the variation of the angle of attack $\Delta\alpha$ approaches the limiting value

$$\lim_{\tau \to \infty} \Delta\alpha = -\frac{(0)a_{2\eta}}{(0)a_{2\alpha}} \Delta\eta_{max} \tag{88}$$

In order to satisfy the requirement that an equal multiple of load Δn be obtained for the approximation method, the condition must be fulfilled that for both calculation methods $\Delta\alpha$ tends toward the same limiting value.

If one assumes, therefore, in [52] and [69], respectively, that $\tau \longrightarrow \infty$, there follows

$$-\frac{(0)a_{2\eta}}{(0)a_{2\alpha}} \Delta\eta_{max} = \frac{\Delta_2(0)}{D(0)} \Delta\eta_{hmax}$$

or

$$\Delta\eta_{max} = -\frac{(0)a_{2\alpha}}{(0)a_{2\eta}} \frac{\Delta_2(0)}{D(0)} \Delta\eta_{hmax} \tag{89}$$

However, on the other hand

$$\Delta\eta_{max} = (\eta')_{max}\tau_1 \tag{89a}$$

so that τ_1 becomes, because of (86),

$$\tau_1 = -\frac{(0)a_{2\alpha}}{(0)a_{2\eta}}\frac{\Delta_2(0)}{D(0)}\frac{\sqrt{(0)a_{1\eta}}}{C_1}\, e^{-\frac{\kappa_\eta}{\omega_\eta}\arctan\left(-\frac{\omega_\eta}{\kappa_\eta}\right)} \tag{90}$$

If one interprets the main control surface variation represented in figure 31 as superposition of the two deflection phenomena

$$\Delta\eta(\tau) = (\eta')_{max}\tau \qquad \text{for} \quad 0 \leqq \tau < \infty$$

and

$$\Delta\eta(\tau) = \begin{cases} 0 & \text{for} \quad 0 \leqq \tau < \tau_1 \\ -(\eta')_{max}(\tau - \tau_1) & \text{for} \quad \tau_1 \leqq \tau < \infty \end{cases}$$

there results as solution of (87) the relation

$$\Delta\alpha = -\frac{(0)a_{2\eta}}{(0)a_{2\alpha}}\Delta\eta_{max}\left[1 + \left\{d_o \sin\omega_\alpha\tau + d_1\cos\omega_\alpha\tau\right\}e^{\kappa_\alpha\tau}\right]$$

or, taking (89) into account and after division by $\Delta\eta_{hmax}$

$$\frac{\Delta\alpha}{\Delta\eta_{hmax}} = \frac{\Delta_2(0)}{D(0)}\left[1 + \left\{d_o \sin\omega_\alpha\tau + d_1\cos\omega_\alpha\tau\right\}e^{\kappa_\alpha\tau}\right] \tag{91}$$

with

$$\Delta_2(0) = \begin{vmatrix} (0)a_{1_\eta} & C_1 \\ (0)a_{2_\eta} & C_2 \end{vmatrix}$$

$$D(0) = \begin{vmatrix} (0)a_{1_\eta} & (0)a_{1\alpha} \\ (0)a_{2_\eta} & (0)a_{2\alpha} \end{vmatrix}$$

$$\left.\begin{aligned} d_o &= \frac{1}{\tau_1}\left[-\frac{1}{\omega_\alpha}\left(1 - e^{-\kappa_\alpha \tau_1}\cos \omega_\alpha \tau_1\right) - \frac{(1)a_{2\alpha}}{(0)a_{2\alpha}} e^{-\kappa_\alpha \tau_1}\sin \omega_\alpha \tau_1\right] \\ d_1 &= \frac{1}{\tau_1}\left[\frac{(1)a_{2\alpha}}{(0)a_{2\alpha}}\left(1 - e^{-\kappa_\alpha \tau_1}\cos \omega_\alpha \tau_1\right) - \frac{1}{\omega_\alpha} e^{-\kappa_\alpha \tau_1}\sin \omega_\alpha \tau_1\right] \\ \kappa_\alpha &= -\frac{(1)a_{2\alpha}}{2} \\ \omega_\alpha &= \sqrt{(0)a_{2\alpha} - \left(\frac{(1)a_{2\alpha}}{2}\right)^2} \end{aligned}\right\} \quad (91a)$$

and for the rate of change of the angle-of-attack

$$\frac{\alpha'}{\Delta\eta_{hmax}} = \frac{\Delta_2(0)}{D(0)}\left[d_o' \sin \omega_\alpha \tau + d_1' \cos \omega_\alpha \tau\right] e^{\kappa_\alpha \tau} \quad (92)$$

with

$$\left.\begin{aligned} d_o' &= \kappa_\alpha d_o - \omega_\alpha d_1 \\ d_1' &= \omega_\alpha d_o + \kappa_\alpha d_1 \end{aligned}\right\} \quad (92a)$$

it has to be noted that these solutions are valid only in the interval $\tau_1 \leqq \tau < \infty$.

Since in practice the wing unit as well as the horizontal tail stresses are of importance only for $\tau \geqq \tau_1$, because for $\tau < \tau_1$ only smaller stresses are possible, the equations (91) and (92) are sufficient for the determination of the desired quantities.

In figure 32 the horizontal tail loads as they result for time-dependent tab deflection and according to the approximation method described above are compared once more.

As a conclusion it may be stated that for the design of tab-controlled airplanes this calculation method may be applied for the determination of the wing and horizontal tail loads which is much simpler than that of consideration of the degrees of freedom α and η.

VI. SUMMARY

Continuing the theoretical investigations of the first partial report, FB 2000, the present report discusses the conditions to be expected for an airplane controlled by tabs.

Apart from a compilation of the stability criteria, the influence of variable main-control-surface damping, as well as of variable mass of the main and auxiliary control surfaces, on the frequencies and dampings is observed.

For evaluation of the control effectiveness a comparison is made between the starting phenomena for instantaneous and time-dependent tab and for instantaneous and time-dependent main-control-surface deflection. The increase in control-surface effectiveness by instantaneous tab deflection compared to time-dependent tab deflection is insignificant.

In the representation of the solutions in closed form one has a simple graphical means of observing the variation of the angle of attack for control displacement and subsequent control restoration, which simultaneously represents a measure for the wing stresses.

The most favourable utilization of material for fuselage and horizontal tail is obviously accomplished when their strength is determined in relation to that of the wing unit. For the structural aspects of fuselage and horizontal tail the peak values of the horizontal tail load ΔP_{H_1} in control displacement and ΔP_{H_2} in control restoration are decisive; they also are best determined graphically. This method permits at the same time the envelope of all possible peak values ΔP_{H_2} to be given.

The discussion of the amplitude and phase displacement functions for periodic excitations of the tabs demonstrates impressively the influence of variable main-control-surface damping. Since for normal control surfaces the damping coefficient $^{(1)}a_{1\eta}$ will, at this point, due to air forces, lie in the order of magnitude of $0.3 < {}^{(1)}a_{1\eta} < 0.5$, that is, in the neighborhood of aperiodically oscillating motions, additional damping may be foregone. Nevertheless it will be advisable to avoid periodic excitations, for instance by engine vibrations.

For preliminary calculation of wing and horizontal tail stresses in airplane designing a simpler calculation method than can be used when the two degrees of freedom α and η are taken into consideration is desirable.

It is shown that a good approximation of the wing-unit as well as of the horizontal tail stresses is obtained when the variation of the main-control-surface deflection is idealized in such a manner that the variation increases linearily up to a maximum deflection and then remains constant. The maximum deflection velocity is to be determined from the differential equation of the η-coordinate, omitting all α-terms, and the constant main-control-surface deflection is to be fixed so that with $\tau \longrightarrow \infty$ equal multiples of load are obtained for indirect as well as for direct control-surface activation.

Translated by Mary L. Mahler
National Advisory Committee
for Aeronautics

VII. BIBLIOGRAPHY

1. Fuchs–Hopf–Seewald: Aerodynamik. Berlin, Julius Springer, 1934.

2. Klotter, K.: Einführung in die Technische Schwingungslehre I. Berlin, Julius Springer, 1938.

3. Müller–Prange: Allgemeine Mechanik. Leipzig, Dr. Max Jäneke, 1923.

4. Kaul–Lindemann: Vorausberechnung des Lastvielfachen beim Abfangen. FB 510/3. Zur Berechnung der Höhenleitwerkslast bei Höhenruderbetätigung. FB 510/4.

5. Kupper: Ergebnisse von Leitwerkstheorien bei verschwindender Profildicke. Luftfahrtforschung 1943, Bd. 20, pp. 22–28.

6. Kaul–Lindemann: Flugversuche und Rechnungen zur Bestimmung der Luftkraft am Flugzeug bei Höhenruderbetätigung. Jahrbuch 1938 der Deutschen Luftfahrtforschung, pp. 194–205.

7. Routh, John: Die Dynamik der Systeme starrer Körper. Leipzig, B. G. Teubner, 1898.

8. Doetsch, G.: Theorie und Anwendung der Laplace–Transformation. Berlin, Julius Springer, 1937.

9. Glauert, H.: Die Grundlagen der Tragflügel– und Luftschraubentheorie. Berlin, Julius Springer, 1929.

10. Blenk, H.: Über die Schwingungen von Flugzeugen mit freiem Höhenruder. Zeitschrift für Flugtechnik und Motorluftschiffahrt, München and Berlin, Oldenbourg 1933, pp. 365–370.

11. Schmidt, H.: Analysis der elementaren Funktionen und ausgewählte Kapitel der analytischen Mechanik. DVL–Vorlesung, unpublished.

12. Göthert, R.: Systematische Untersuchungen an Flügeln mit Klappen und Hilfsklappen. FB 553a, FB 553b.

TABLE I

THEORETICAL CALCULATIONS OF UNSTEADY FLOW VALUES

[Calculated for $T_0 = T_1 = 67.4^\circ$ F]

$\frac{u_2}{a_0}$	$\frac{p_2}{p_0}$	$\frac{u_2 - a_{22}}{a_0}$	$\frac{W_b}{a_0}$	$\frac{p_2}{p_1}$	$\frac{p_1}{p_0}$	$\frac{p_2 - p_1}{p_0}$	$T_0 - T_{22}$ (°F)	$T_2 - T_1$ (°F)	$\frac{W_c}{a_0}$	$\frac{p_3}{p_2}$	$\frac{p_3}{p_0}$	$\frac{p_3 - p_2}{p_0}$	$T_3 - T_2$ (°F)
[a]0.10	0.868	-0.880	1.062	1.149	0.756	0.112	20.9	21.3	-0.981	1.147	0.994	0.126	21.8
.1445	.816	-.828	1.089	1.223	.667	.148	29.8	30.7	-.9755	1.216	.989	.1755	32.0
.15	.808	-.820	1.094	1.230	.657	.151	31.2	32.2	-.974	1.222	.988	.180	33.2
[a].20	.751	-.760	1.127	1.316	.571	.180	41.4	43.3	-.966	1.302	.979	.227	45.0
.248	.701	-.703	1.159	1.402	.500	.201	51.0	54.2	-.9612	1.380	.968	.266	57.1
.25	.698	-.700	1.161	1.406	.497	.202	51.5	54.6	-.961	1.384	.967	.268	57.3
[a].30	.649	-.640	1.196	1.502	.432	.217	61.4	66.2	-.955	1.469	.953	.304	70.0

[a]Values taken from reference 8.

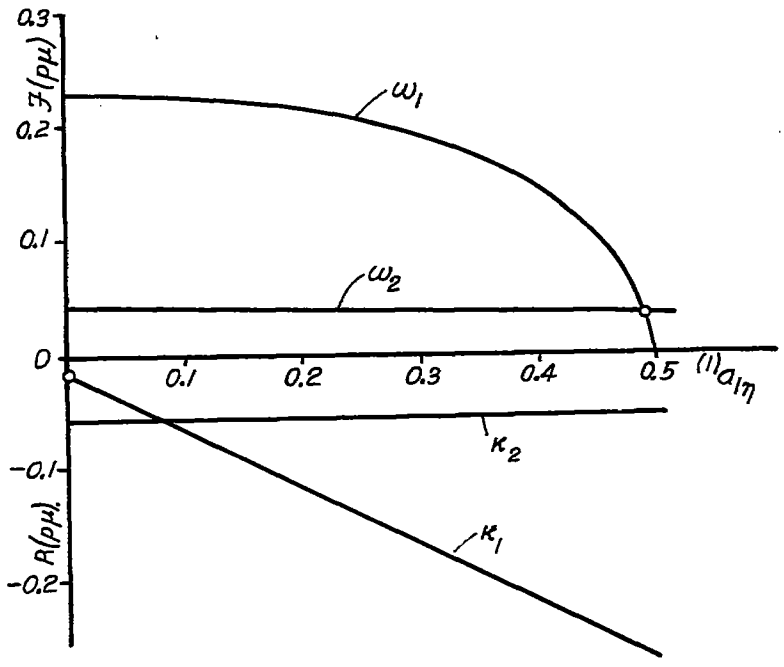

Figure 7.- Real and imaginary part of the roots p_μ as functions of the main-control-surface damping parameter for large flying weight G_{max} of the airplane type Fl_1.

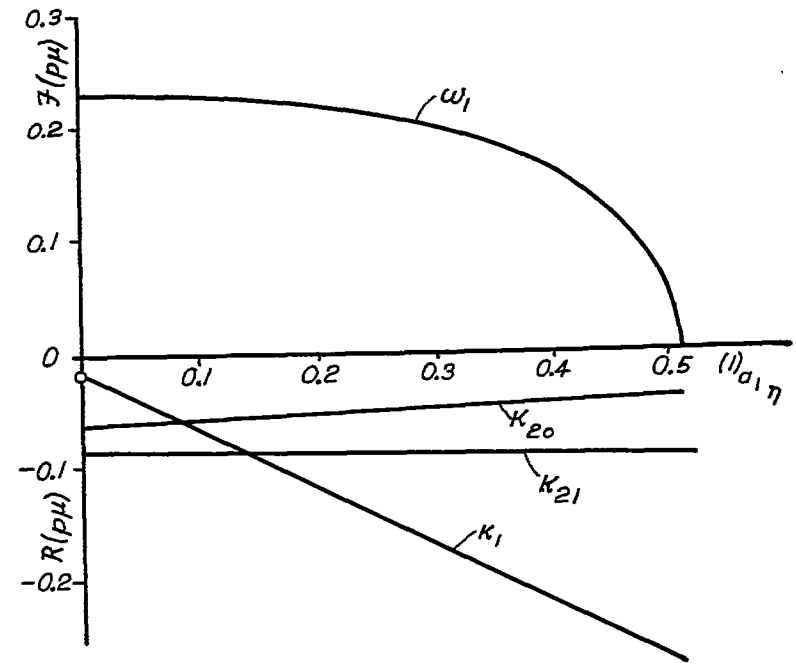

Figure 8.- Real and imaginary part of the roots p_μ as functions of the main-control-surface damping parameter for minimum flying weight G_{min} (Fl_1).

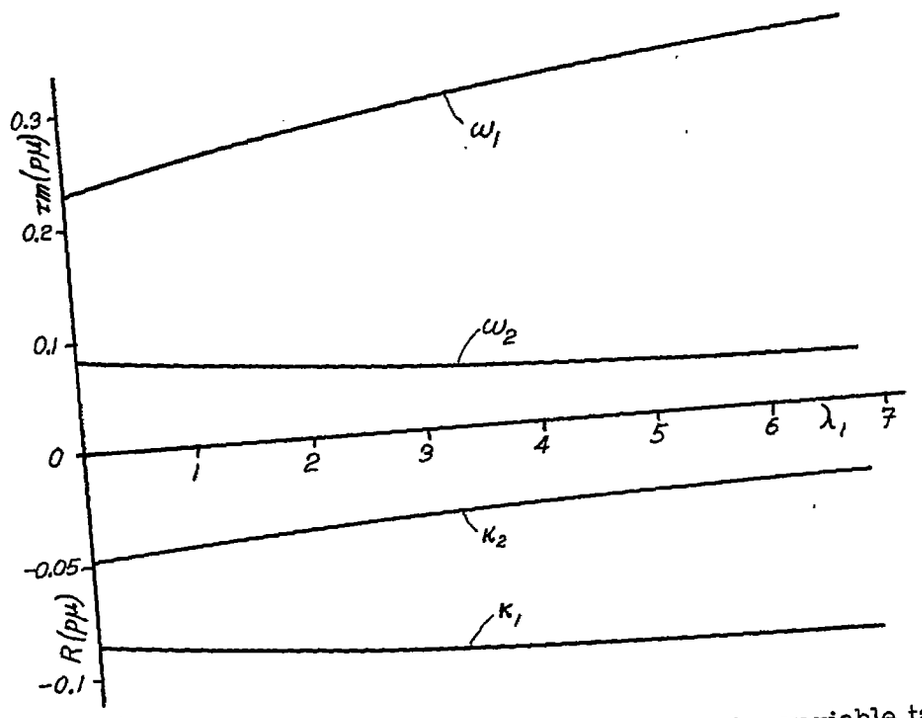

Figure 9.- Real and imaginary parts of the roots p_μ for variable tab mass for the airplane type F_{12}.

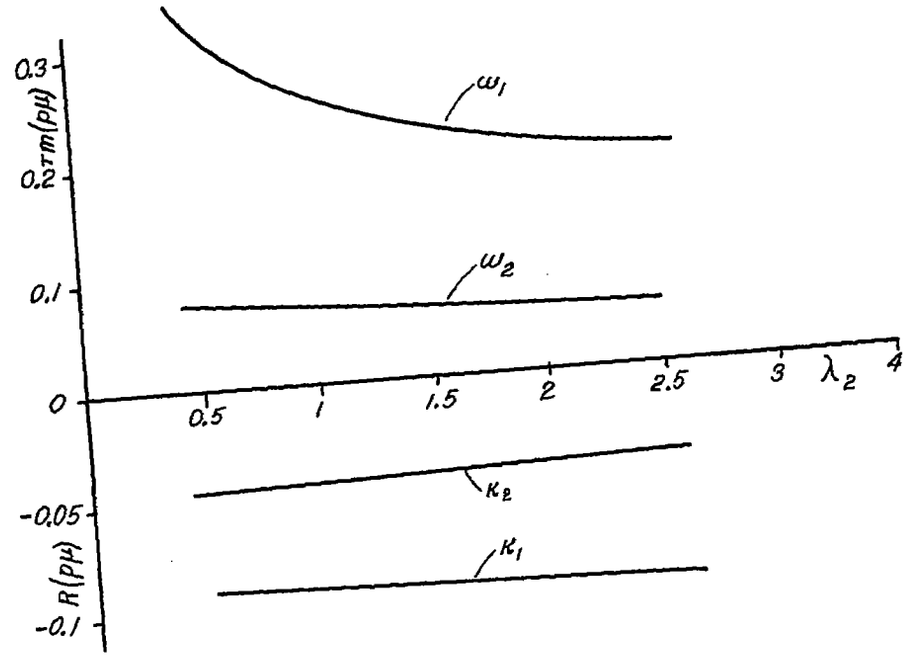

Figure 10.- Real and imaginary parts of the roots p_μ for variable main-control-surface mass for the airplane type F_{12}.

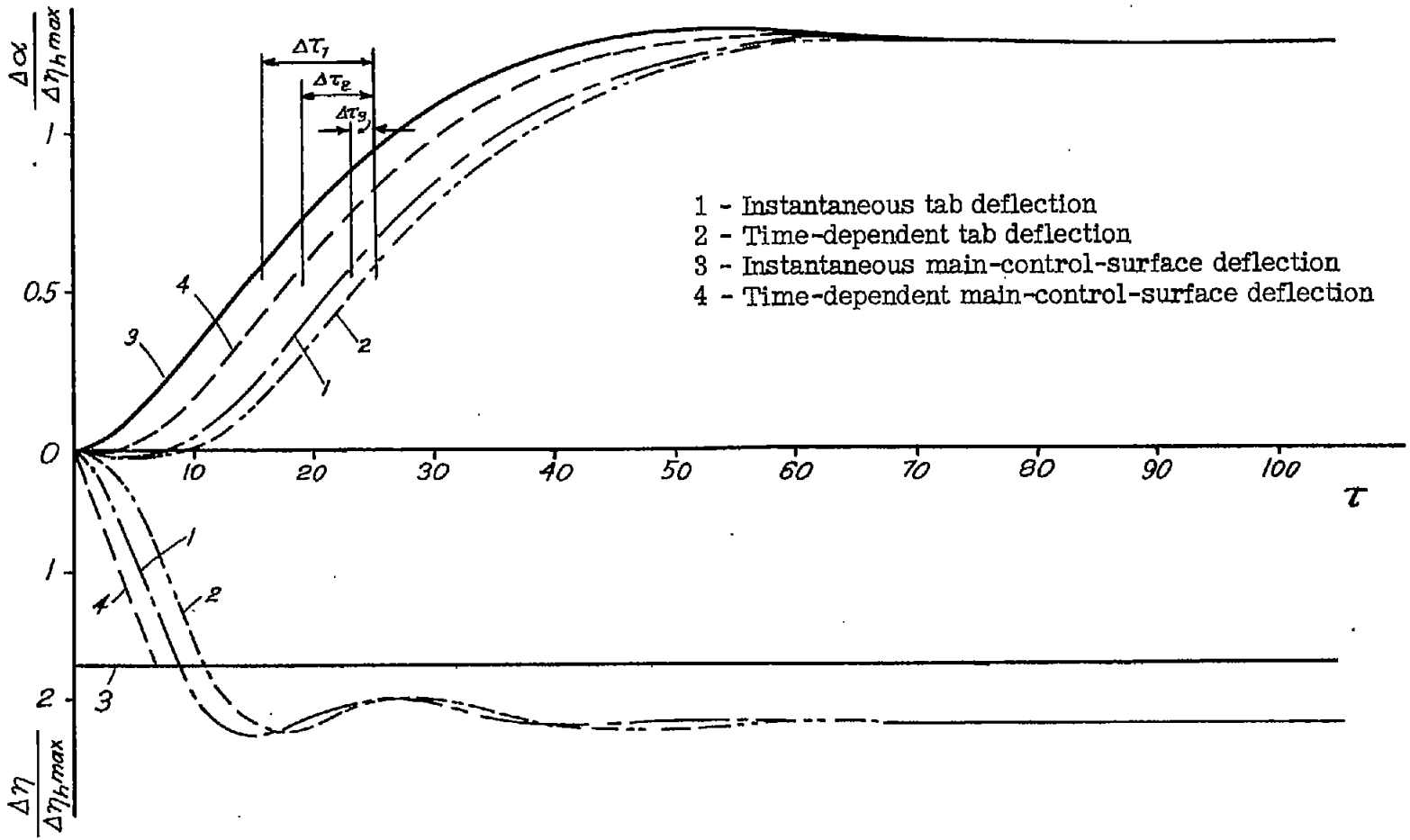

Figure 11.- Comparison of the main-control-surface variation and the variation of the angle of attack for instantaneous and time-dependent tab deflection and for instantaneous and time-dependent main-control-surface deflection, respectively (F'_1).

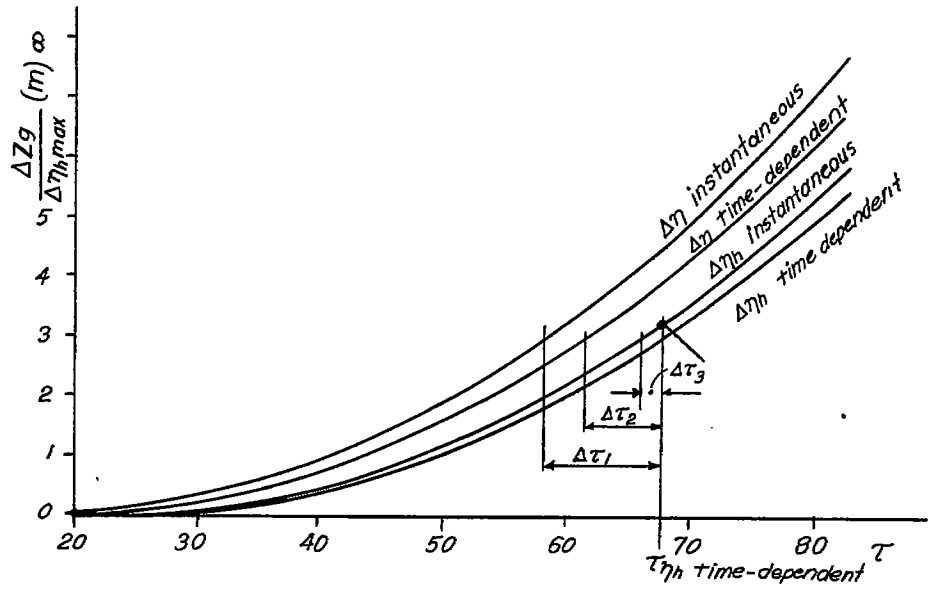

Figure 12.- Obtainable changes in altitude ΔZ_g for different deflection possibilities ($F\tau_1$).

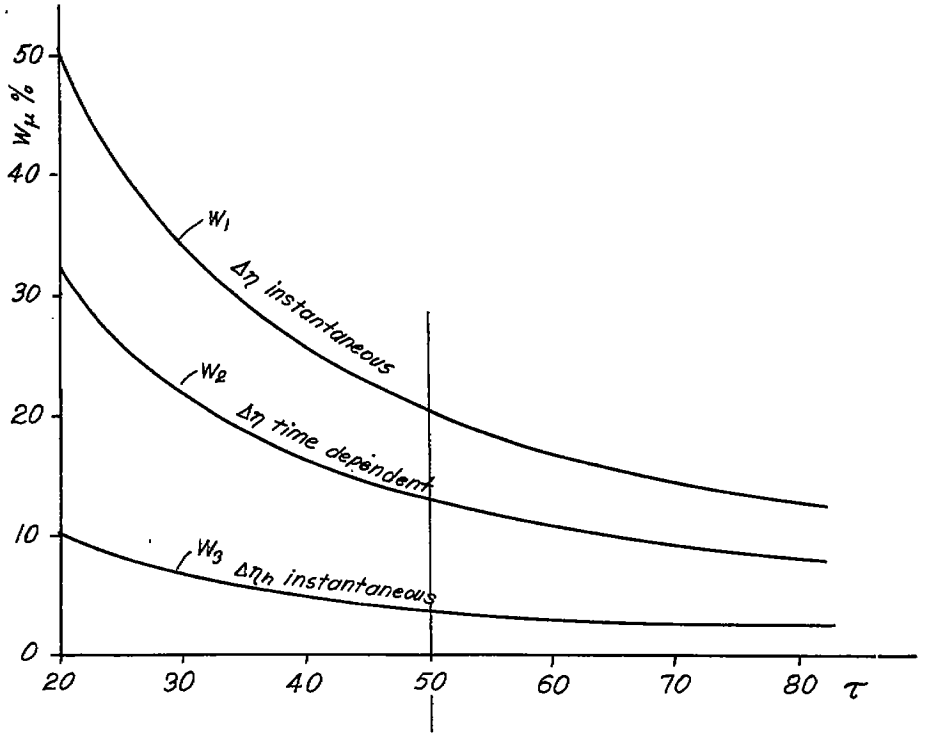

Figure 13.- Increases in control effectiveness for different deflection possibilities ($F\tau_1$).

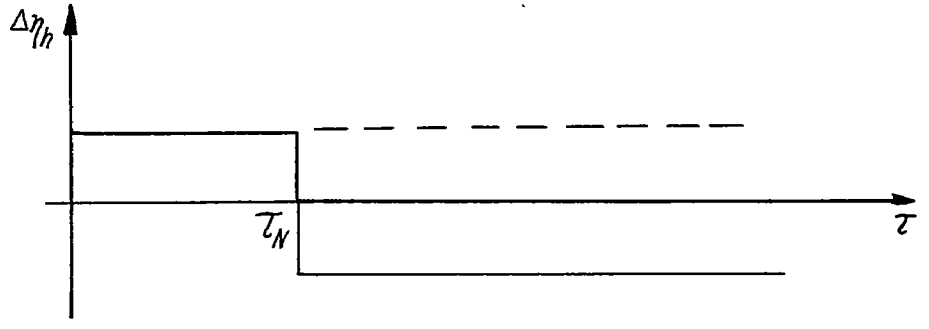

Figure 14.- Superposition of two constant tab deflection phenomena.

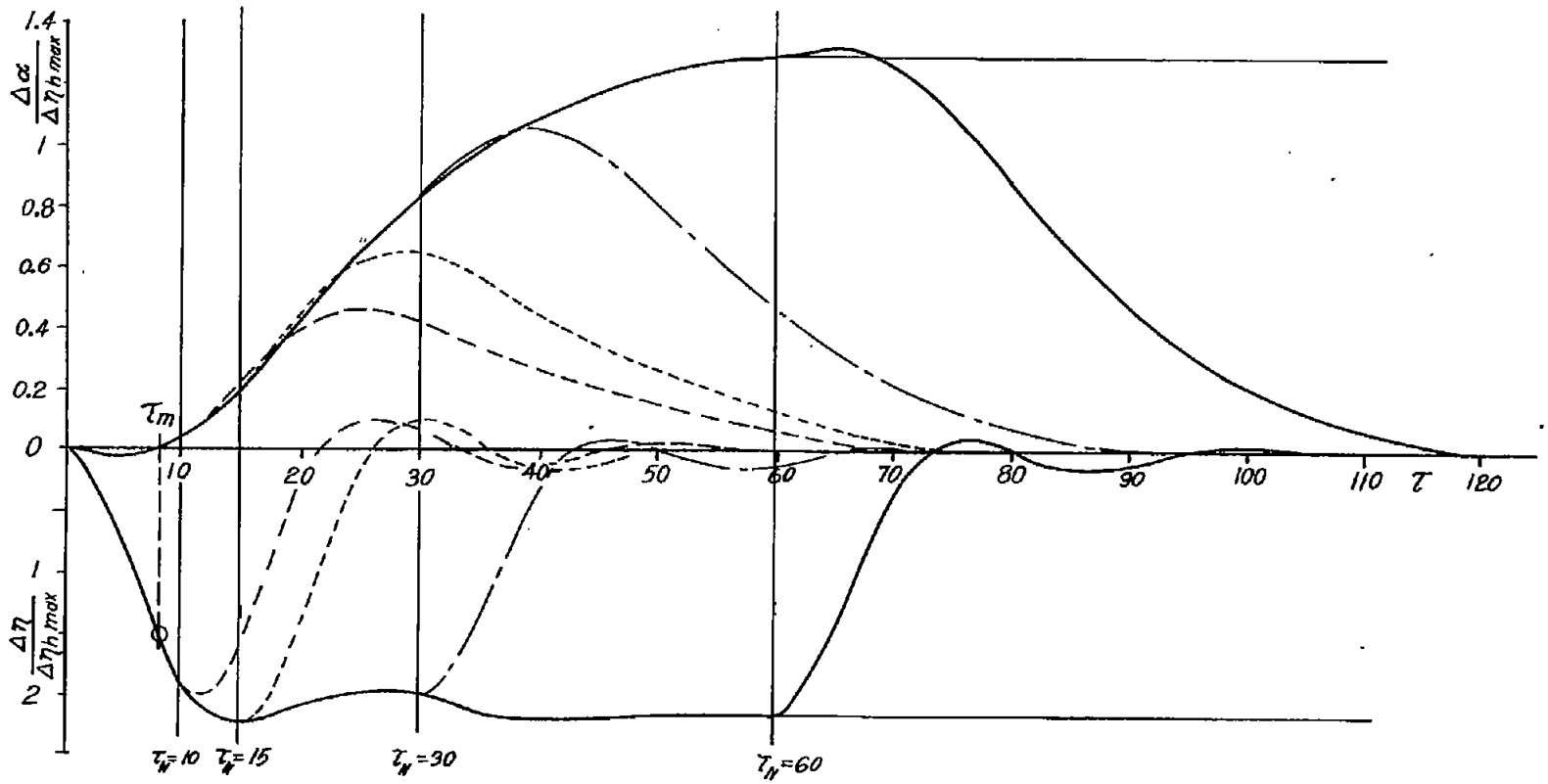

Figure 15.- Control displacement and restoration for instantaneous tab deflection (F_1).

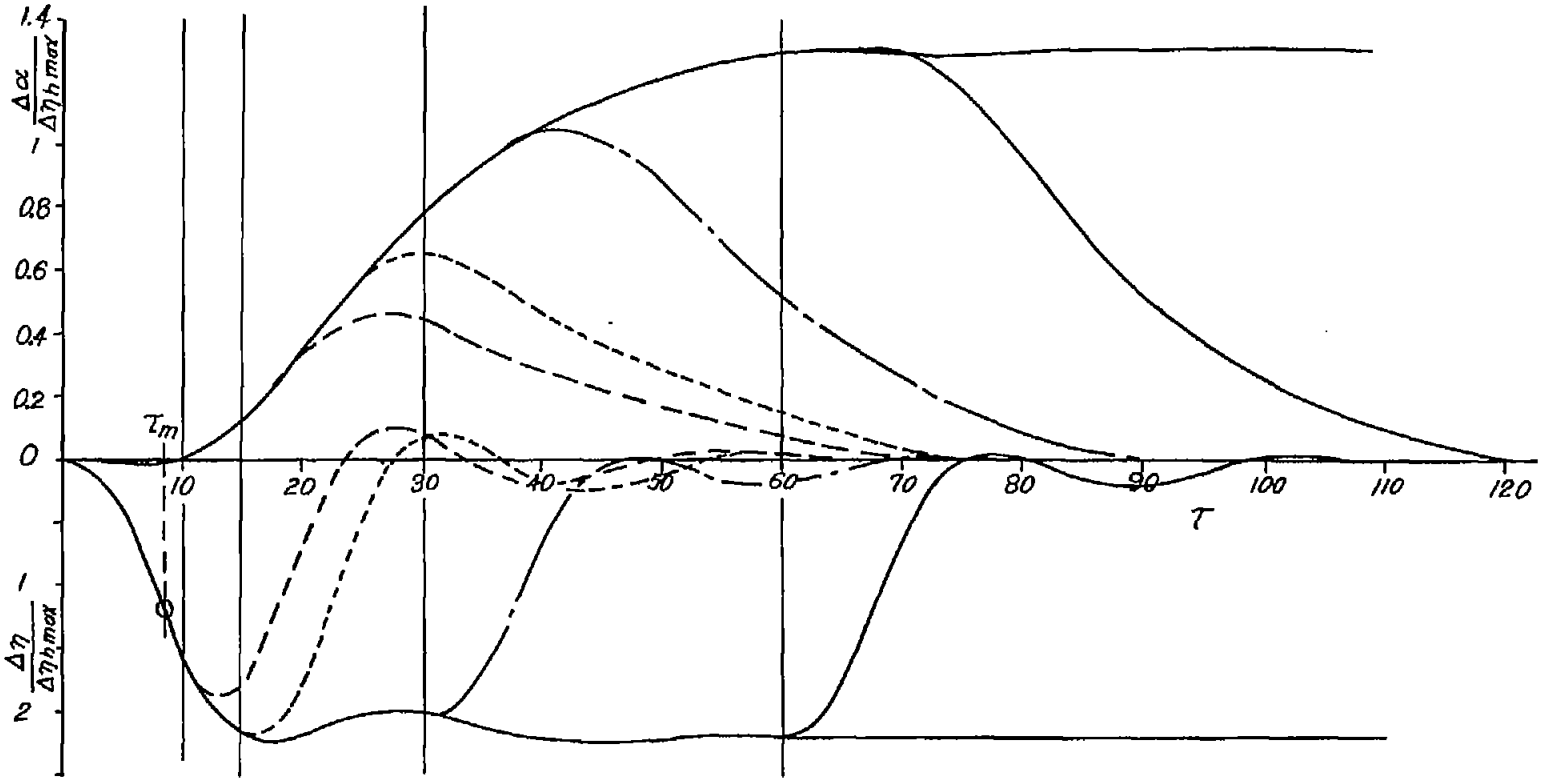

Figure 16.- Control displacement and restoration for time-dependent tab deflection (Fl_1).

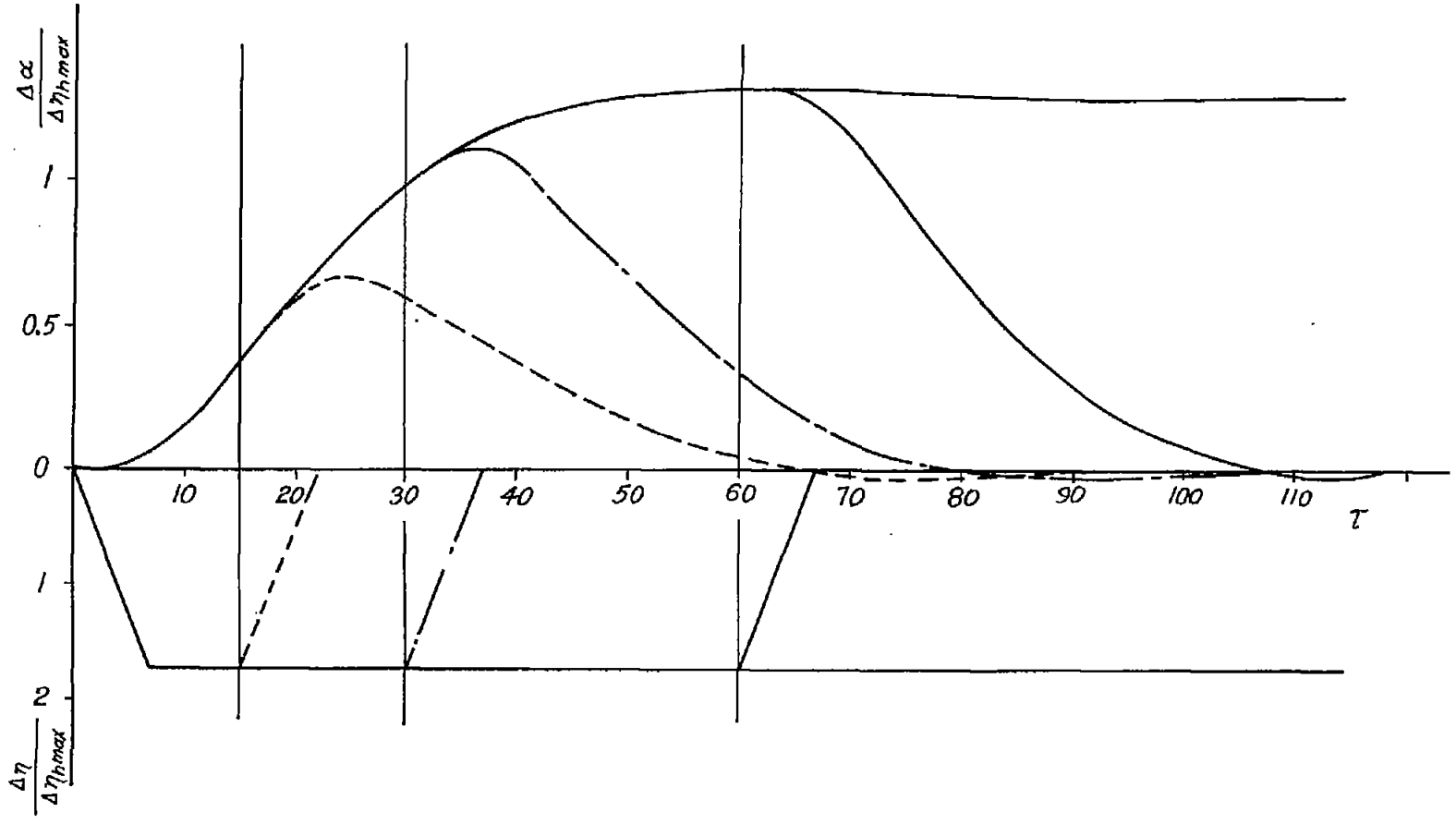

Figure 17.- Control displacement and restoration for time-dependent main-control-surface deflection (F_{l_1}).

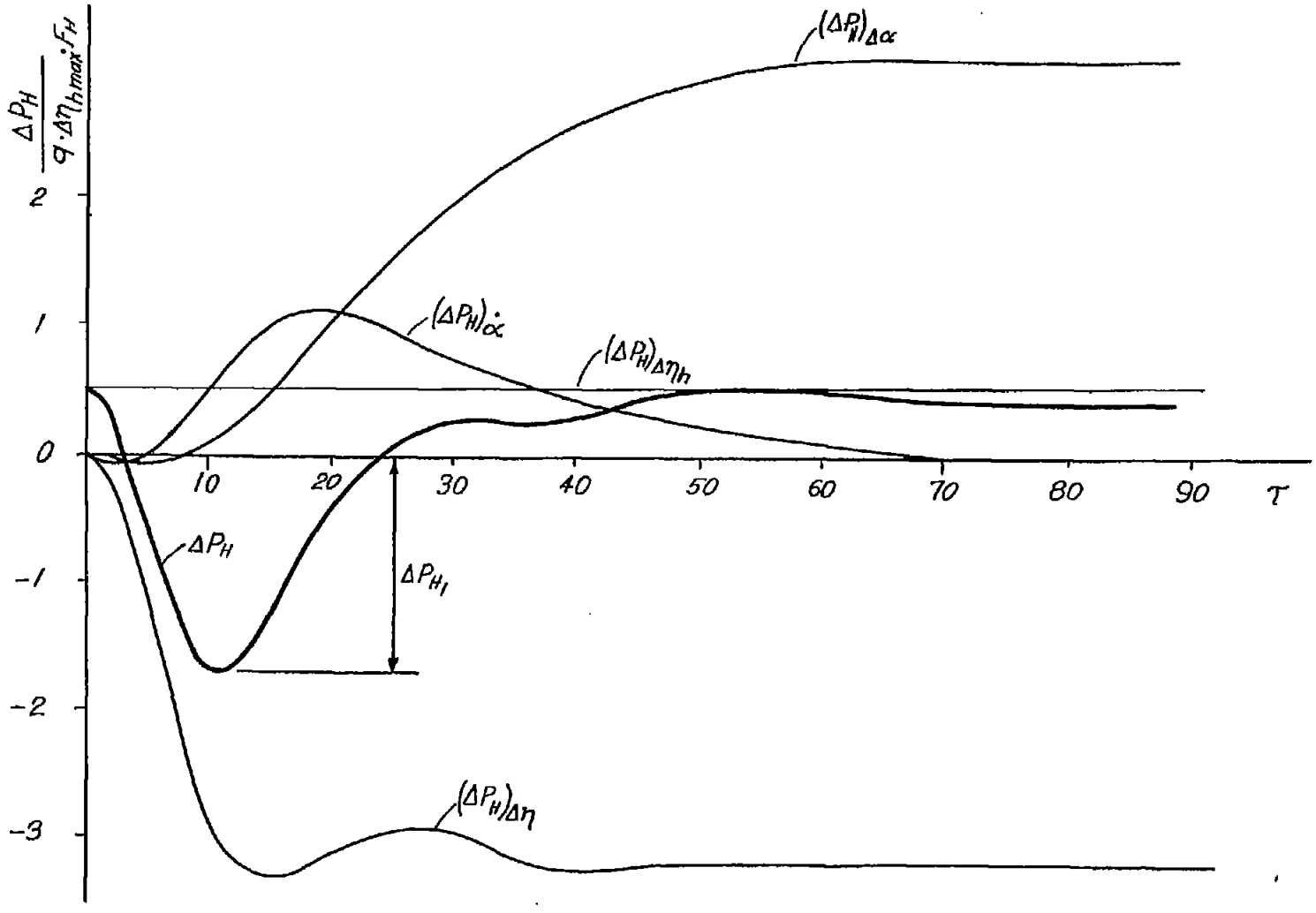

Figure 18.- Horizontal tail loads for control displacement and their components due to $\Delta\alpha$, $\dot{\alpha}$, $\Delta\eta$ and $\Delta\eta_h$ for instantaneous tab deflection ($F\tau_1$).

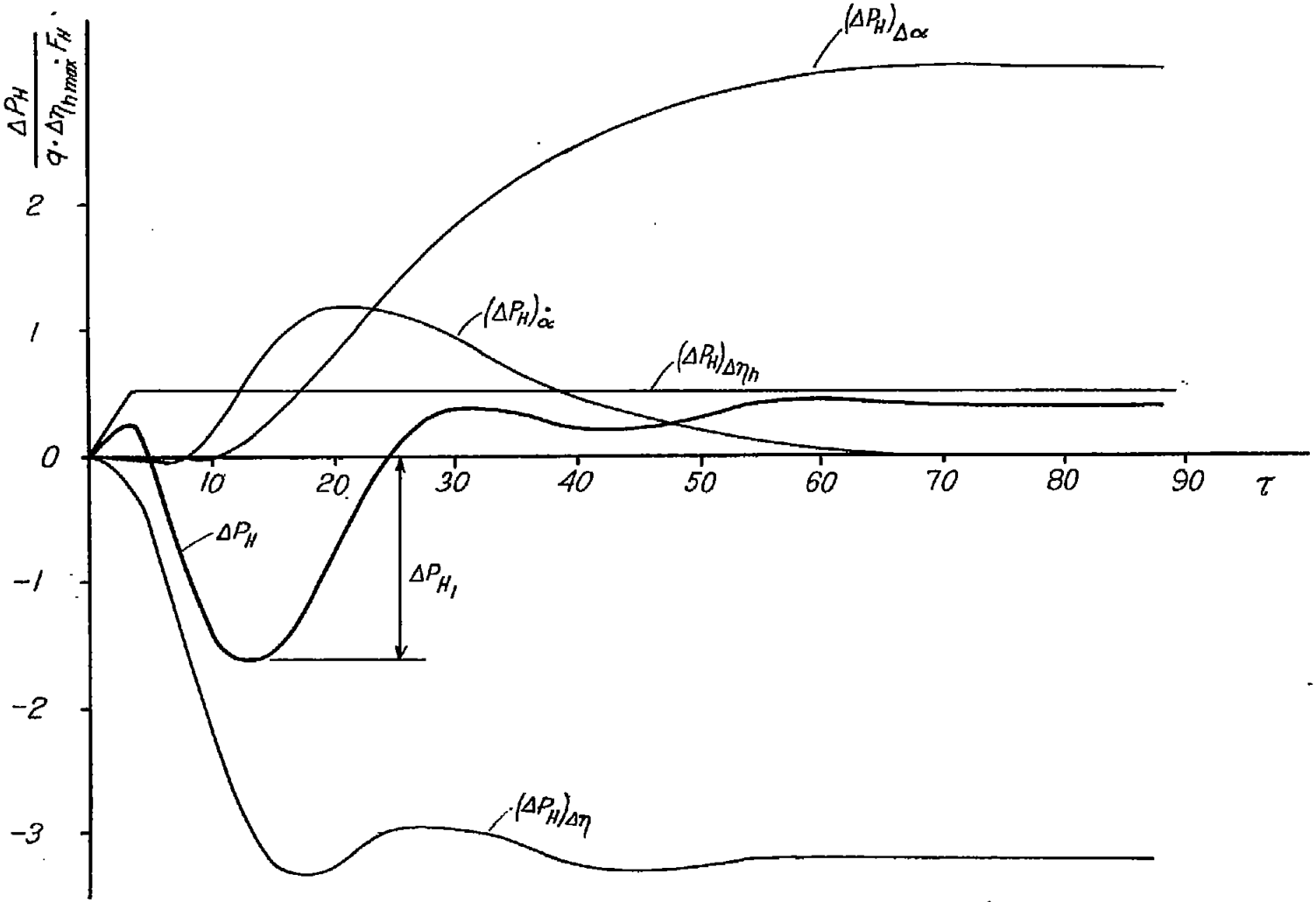

Figure 19.- Horizontal tail loads for control displacement and their components due to $\Delta\alpha$, $\dot{\alpha}$, $\Delta\eta$ and $\Delta\eta_h$ for time-dependent tab deflection ($F\tau_1$).

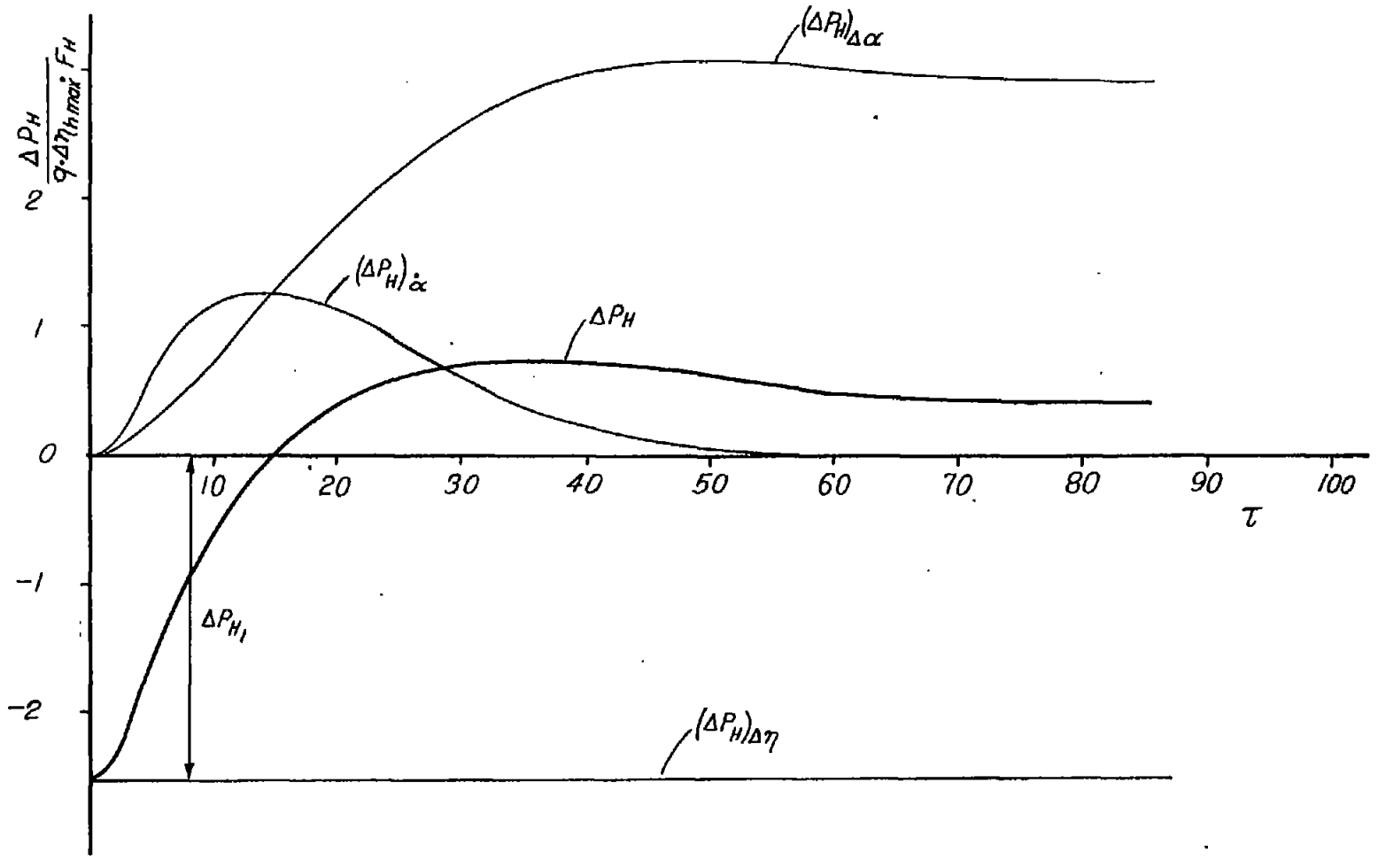

Figure 20.- Horizontal tail loads for control displacement and their components due to $\Delta\alpha$, $\dot{\alpha}$, $\Delta\eta$ and $\Delta\eta_h$ for instantaneous main-control-surface deflection ($F\imath_1$).

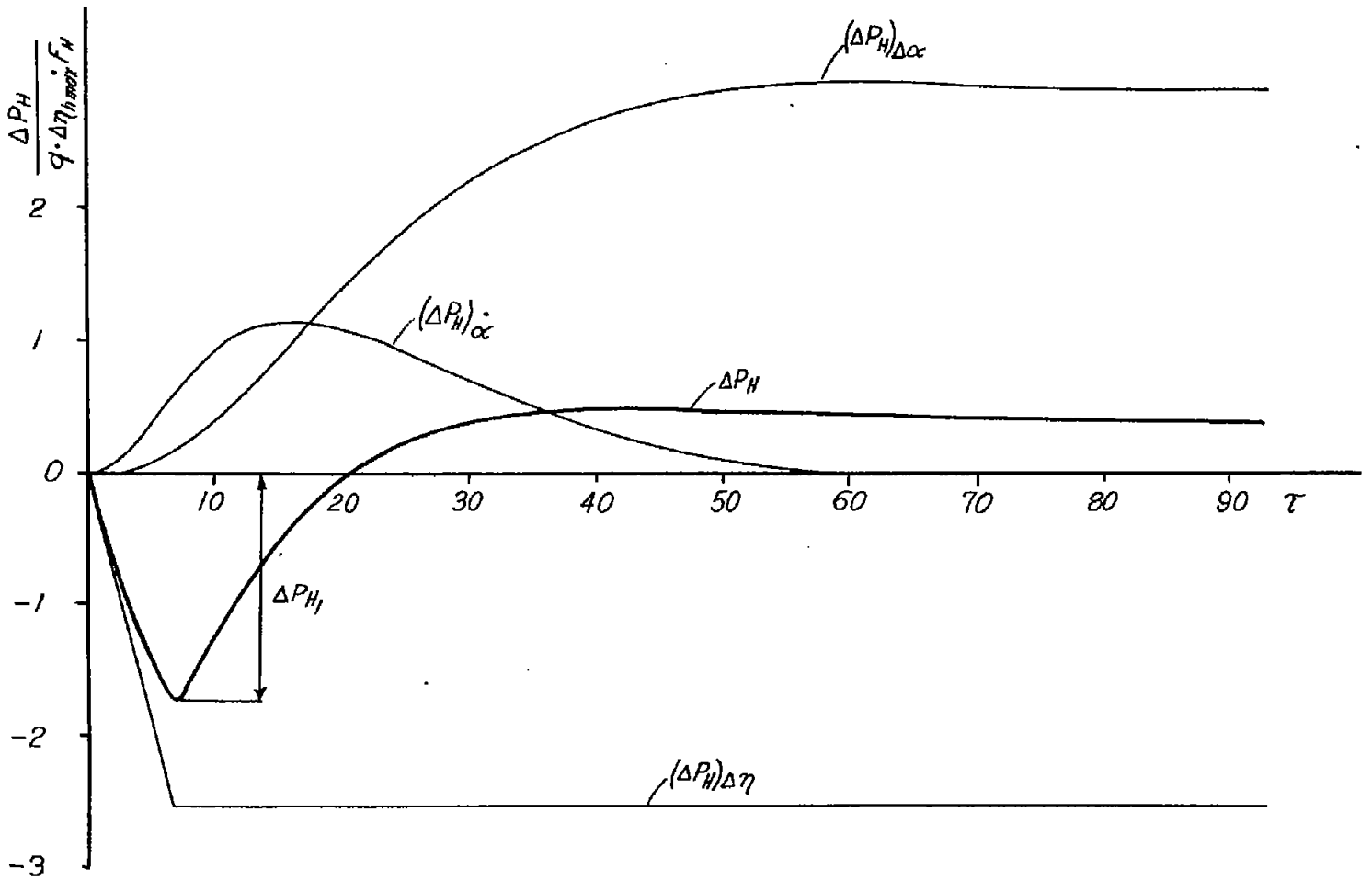

Figure 21.- Horizontal tail loads for control displacement and their components due to $\Delta\alpha$, $\dot{\alpha}$, $\Delta\eta$ and $\Delta\eta_h$ for time-dependent main-control-surface deflection (F_{1_1}).

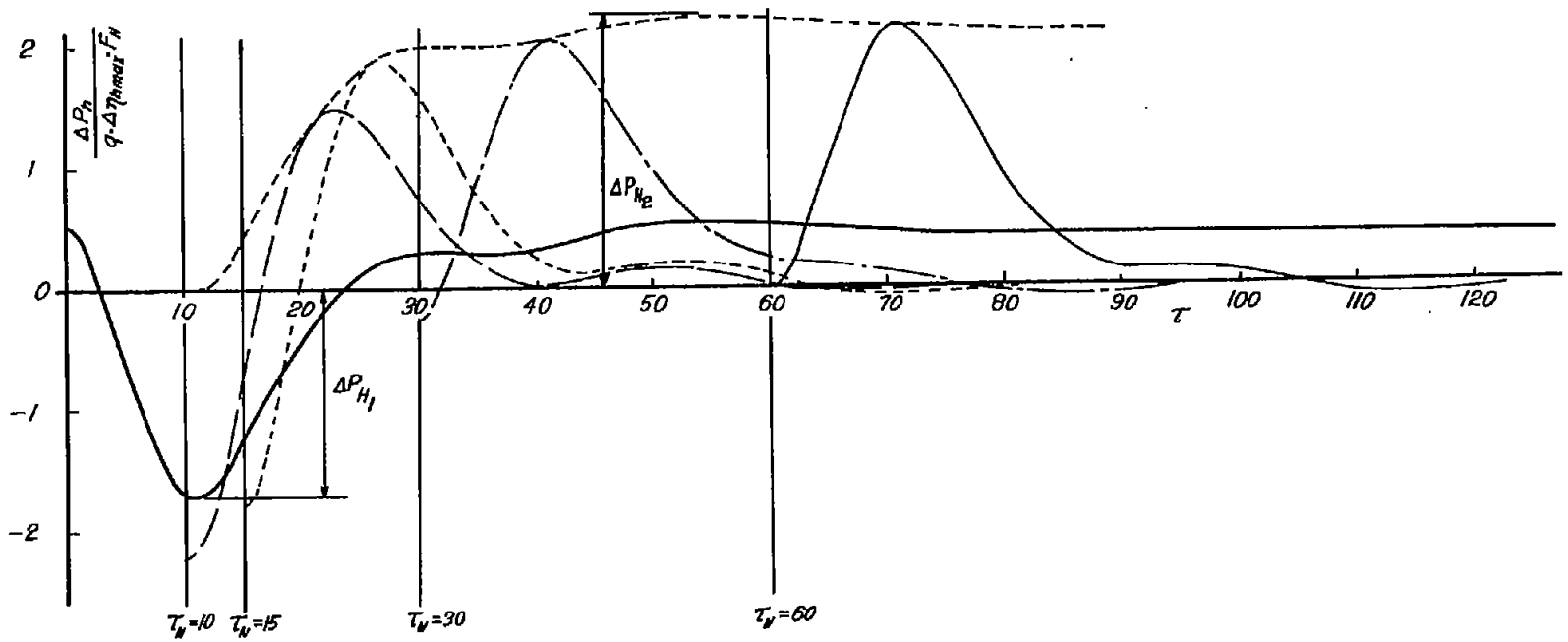

Figure 22.- Horizontal tail loads for control restoration for instantaneous tab deflection (F_{1_1}).

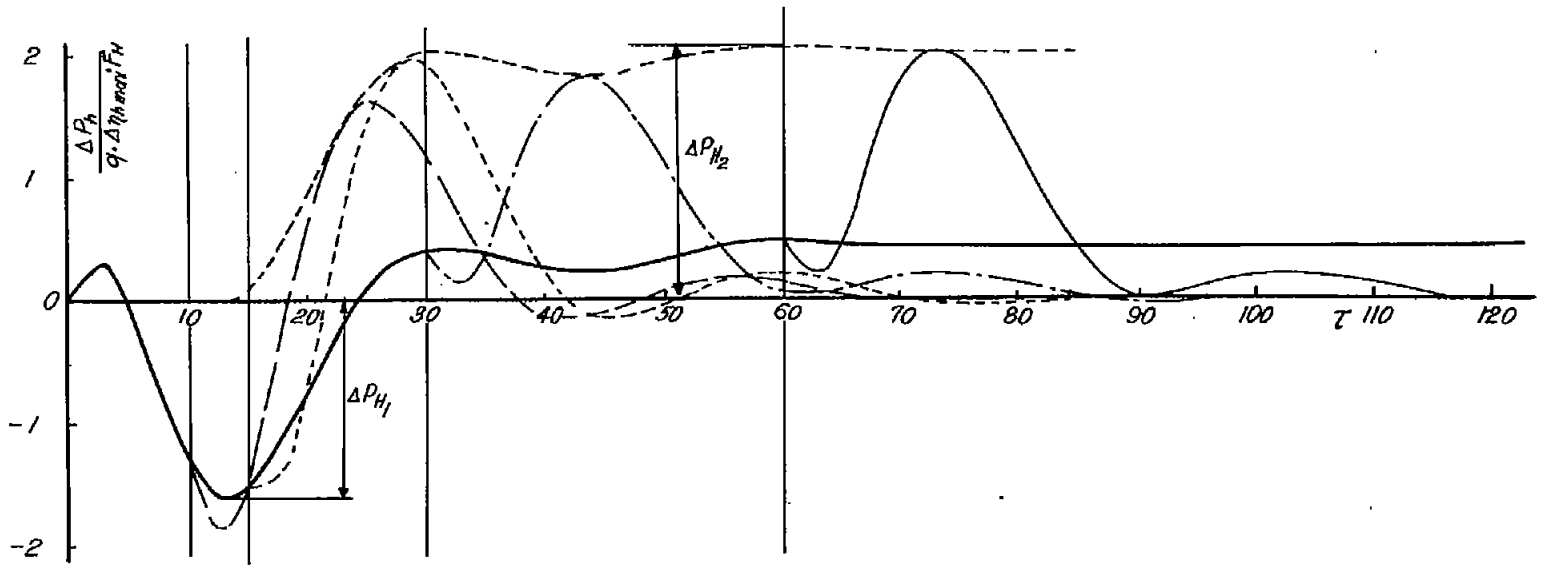

Figure 23.- Horizontal tail loads for control restoration for time-dependent tab deflection (F_{l_1}).

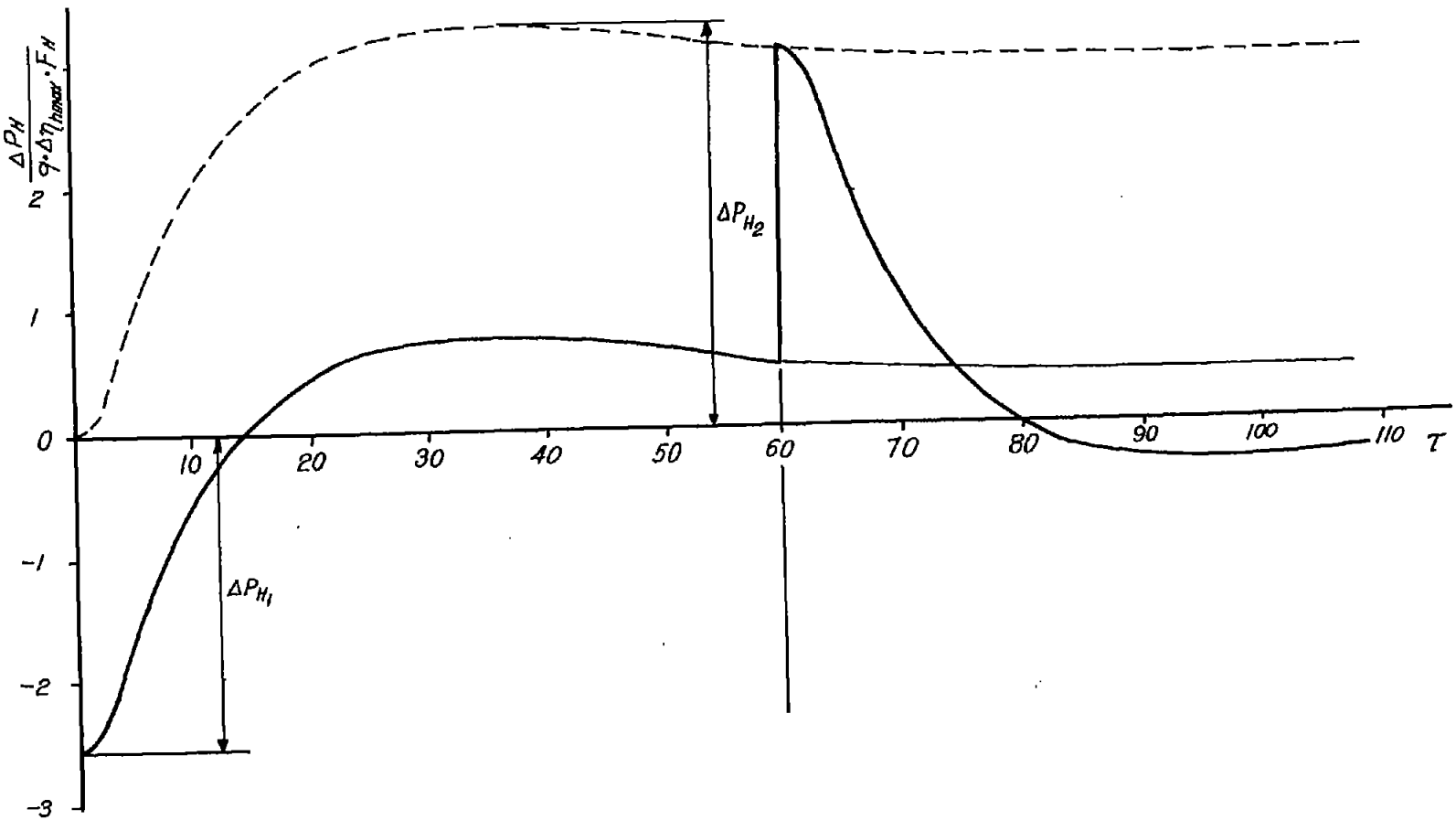

Figure 24.- Horizontal tail loads for control restoration for instantaneous main-control-surface deflection ($F l_1$).

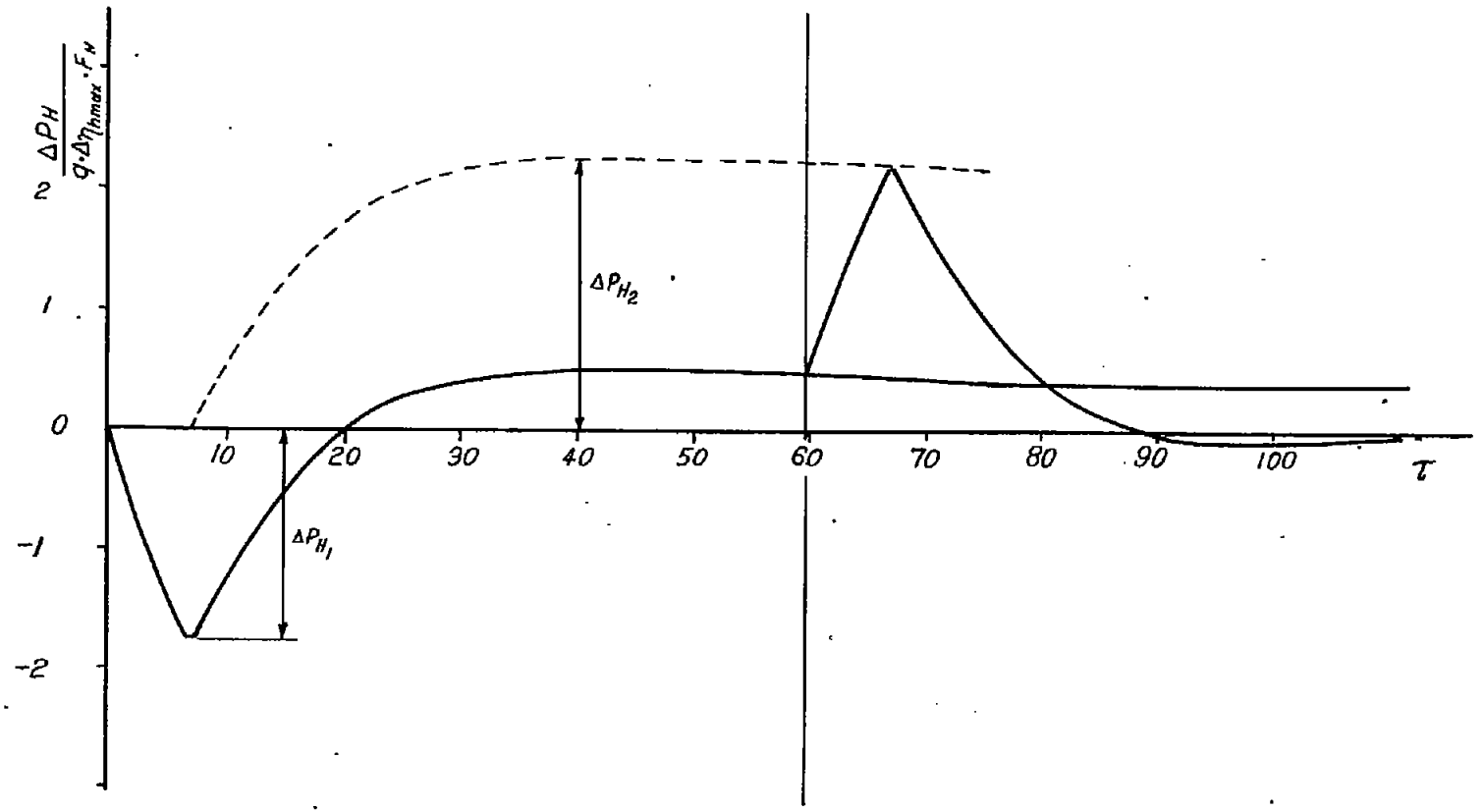

Figure 25.- Horizontal tail loads for control restoration for time-dependent main-control-surface deflection (Fl_1).

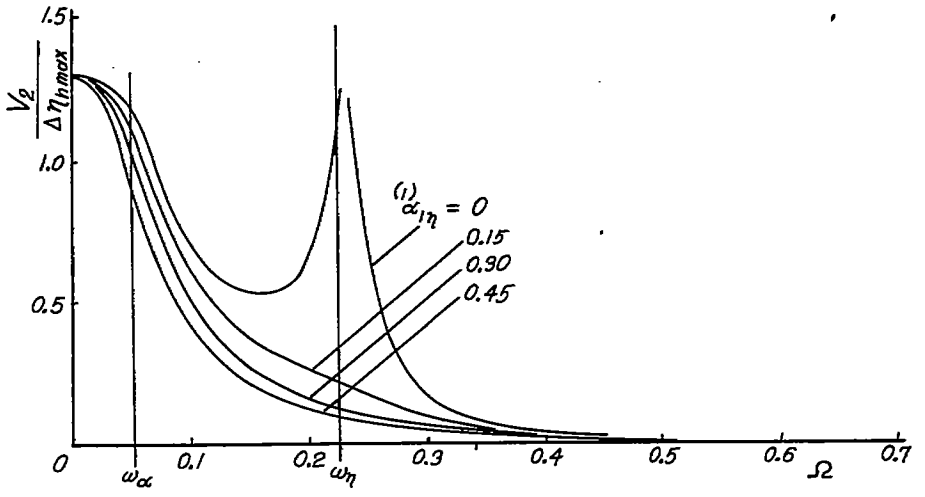

Figure 26.- Amplitude function of the angle of attack due to periodic excitation of the tab (F_1).

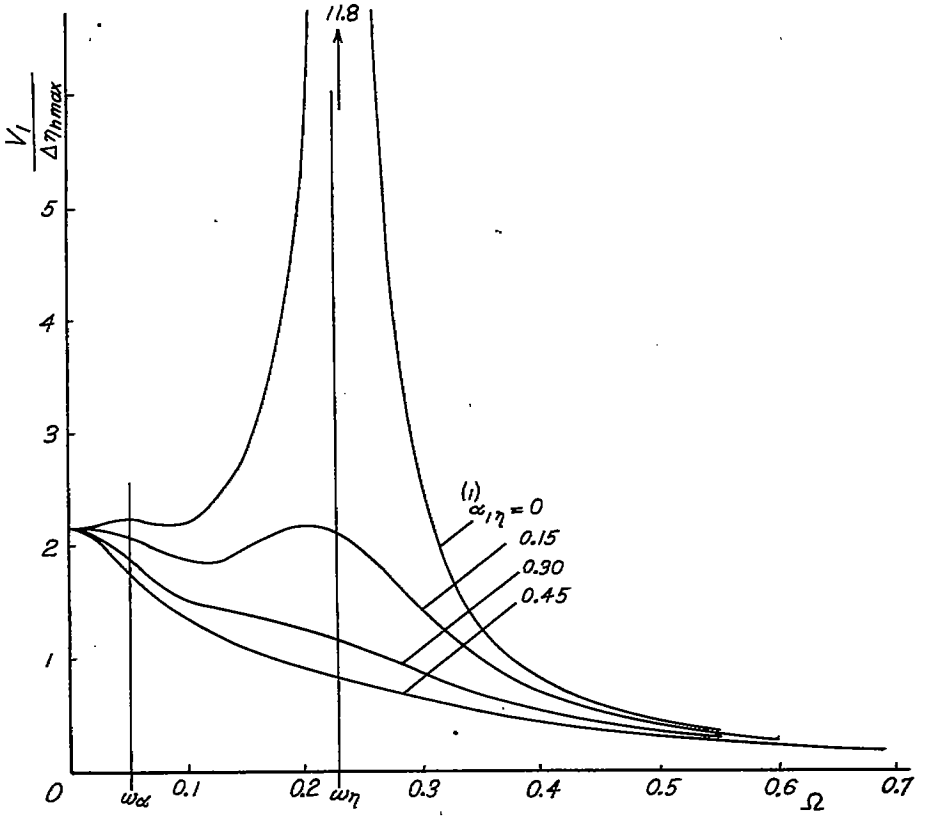

Figure 27.- Amplitude function of the main-control-surface deflection due to periodic excitation of the tab (F_1).

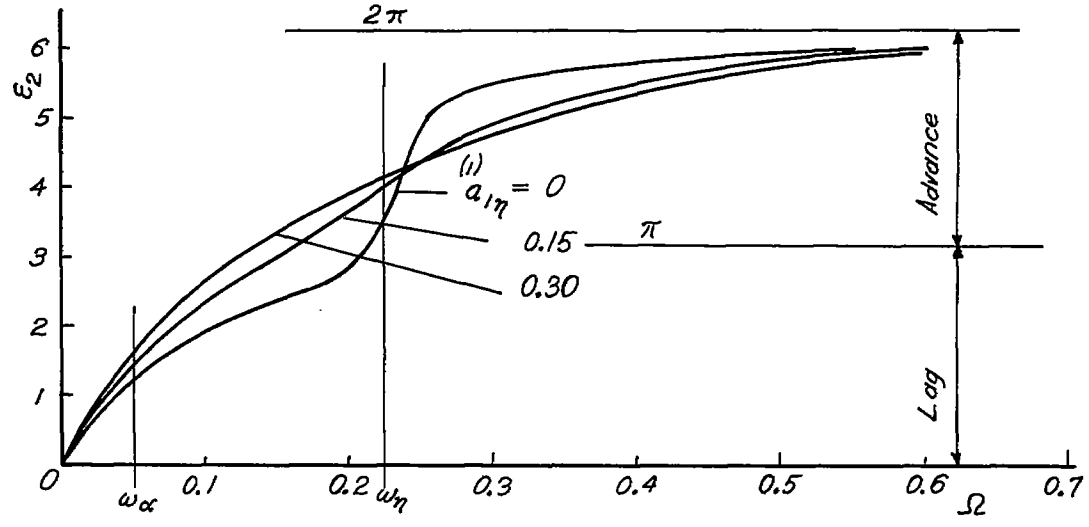

Figure 28.- Phase-displacement functions of the angle of attack due to periodic excitation of the tab (Fl_1).

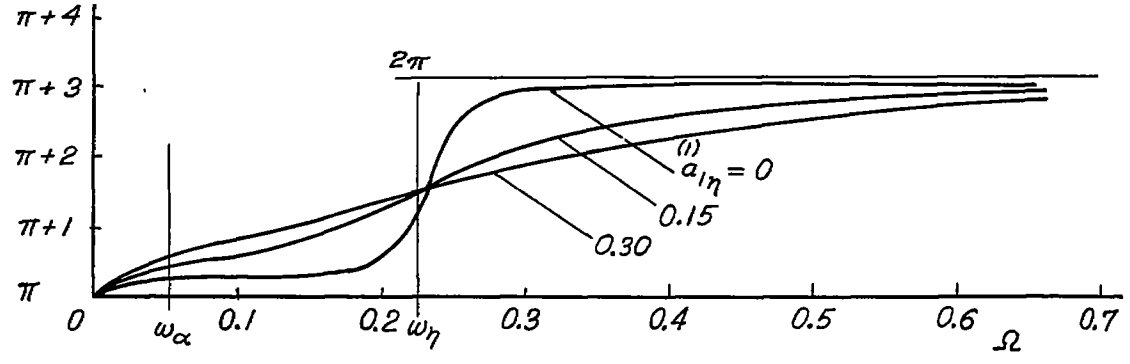

Figure 29.- Phase-displacement functions of the main-control-surface deflection due to periodic excitation of the tab (Fl_1).

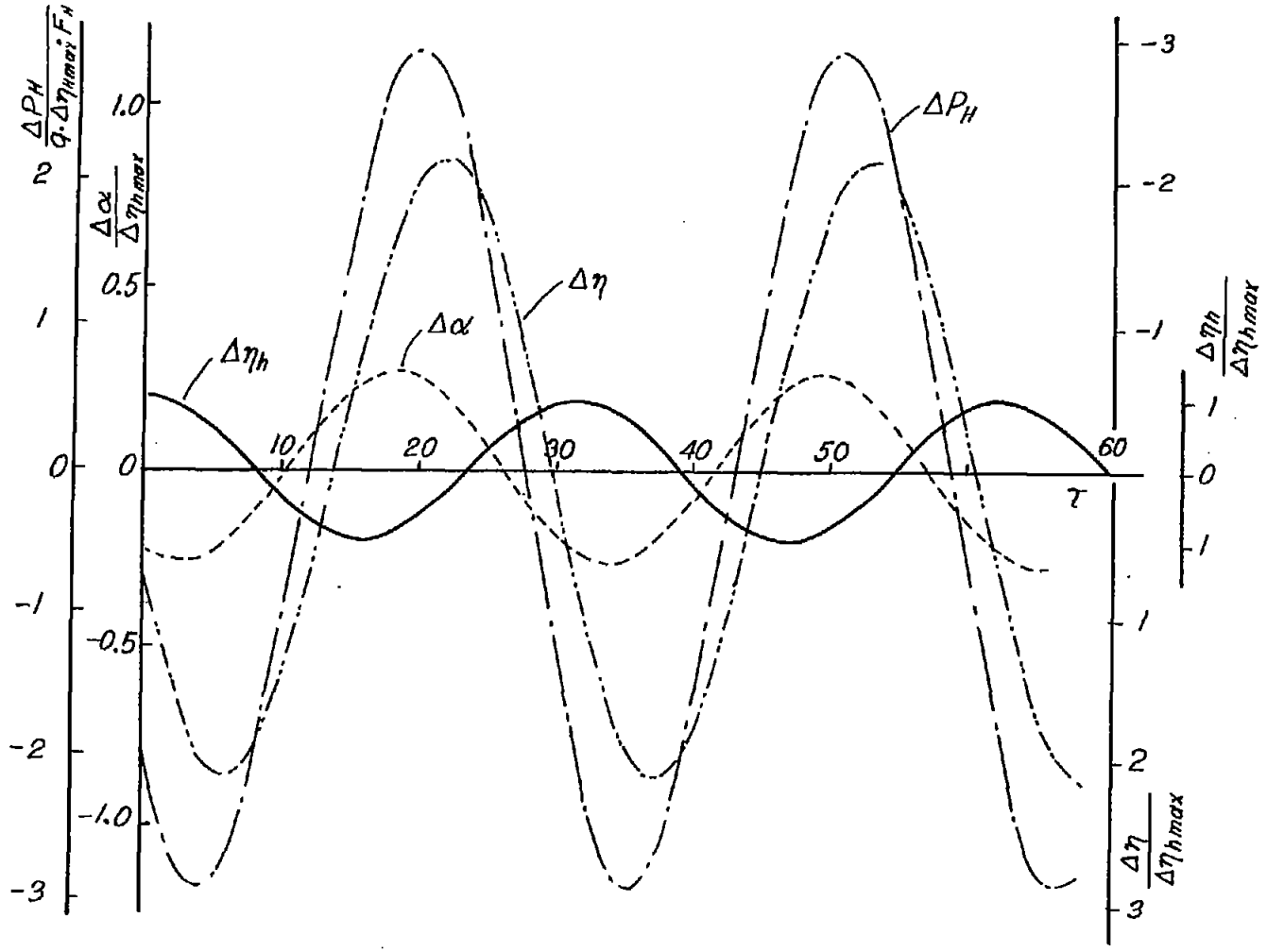

Figure 30.- Variation with time of $\Delta\eta_h$, $\Delta\eta$, $\Delta\alpha$ and ΔP_H for periodic excitation of the tab with a disturbance frequency $\Omega = 0.2$ and a main-control-surface damping parameter $^{(1)}a_{1_\eta} = 0.15$ (Fl_1).

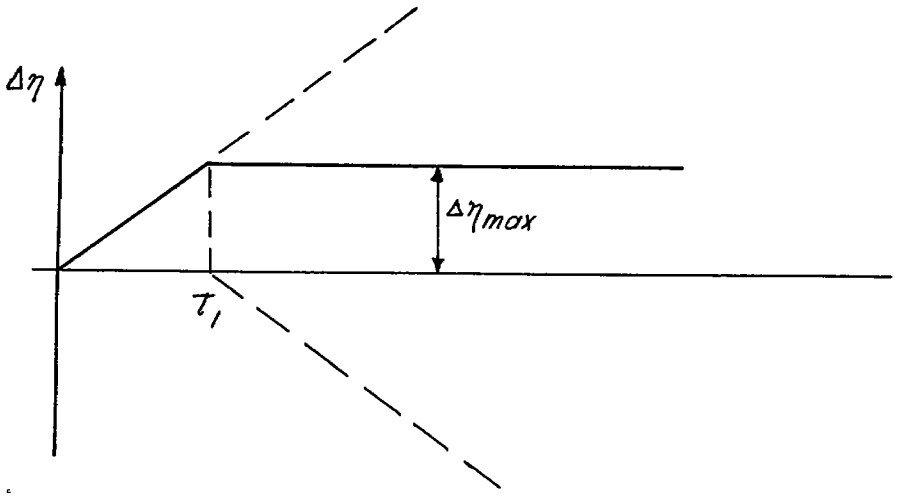

Figure 31.- Idealized main-control-surface variation $\Delta\eta$.

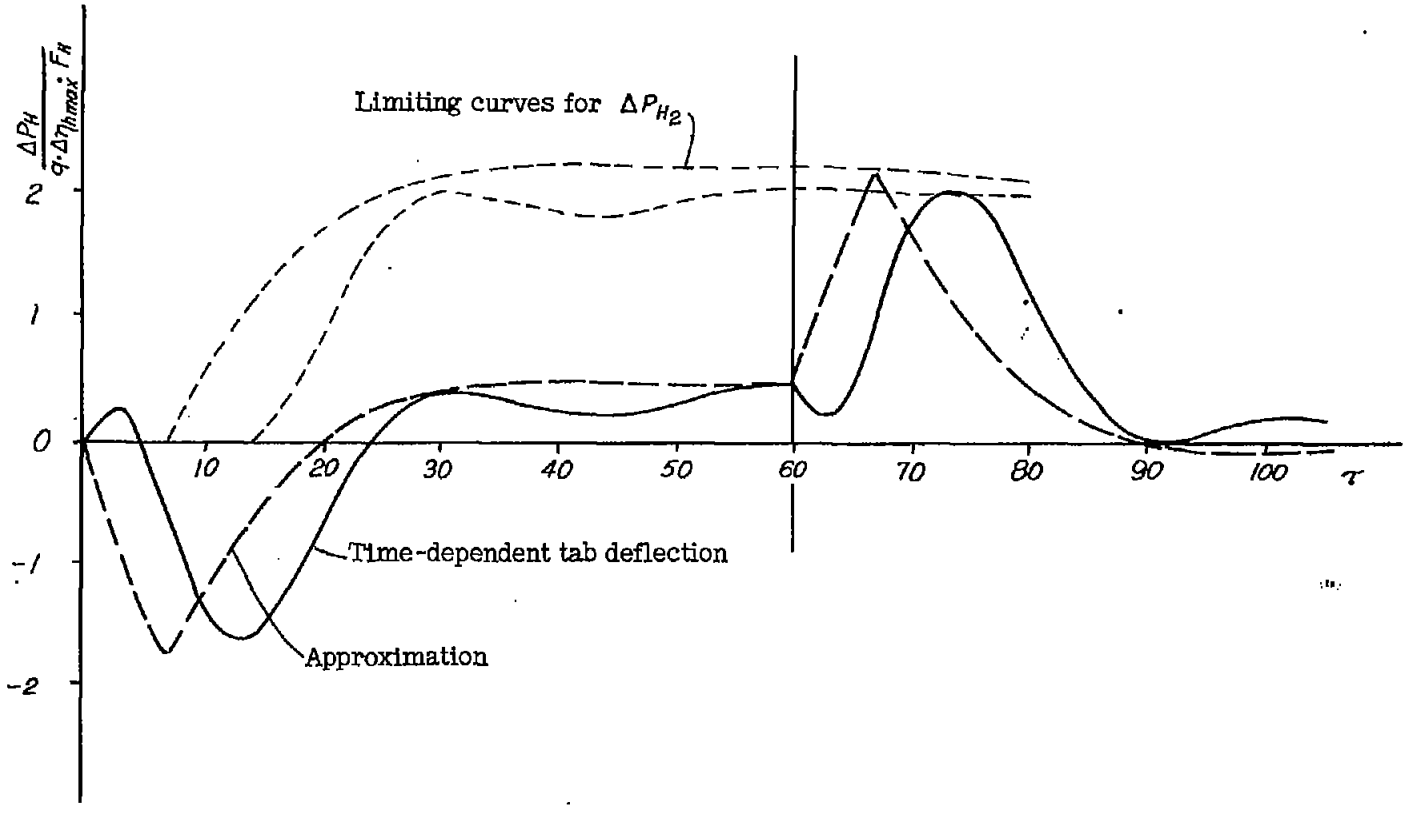

Figure 32.- Comparison of the horizontal tail loads due to time-dependent tab deflection with those determined according to the approximate method.